# 國 立 交 通 大 學

## 應用化學系分子科學碩士班

## 碩 士 論 文

雷射聚焦單一金奈米造成溫度上升引發二維組裝的結構之研究

Two-Dimensional Assembly Formation by Temperature Elevation
upon Tightly Focused Laser Irradiation on a Single Gold Nanoparticle

研 究 生：許 孜瑋 (Tzu-Wei Hsu)

指導教授：三浦 篤志 博士 (Dr. Atsushi Miura)

中華民國一百零一年七月

雷射聚焦單一金奈米造成溫度上升引發二維組裝的結構之研究

# Two-Dimensional Assembly Formation by Temperature Elevation upon Tightly Focused Laser Irradiation on a Single Gold Nanoparticle
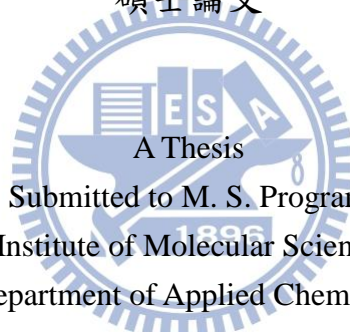
研究生：許孜瑋　　　　　　　Student：Tzu-Wei Hsu

指導教授：三浦篤志 博士　　　Advisor：Dr. Atsushi Miura

國立交通大學
應用化學系分子科學碩士班
碩士論文

A Thesis
Submitted to M. S. Program
Institute of Molecular Science
Department of Applied Chemistry
National Chiao Tung University
In partial Fulfillment of the Requirements
For the Degree of
Master
in

Molecular Science

July 2012

Hsinchu, Taiwan, Republic of China

中華民國一百零一年七月

# 雷射聚焦單一金奈米造成溫度上升引發二維組裝的結構之研究

研究生：許孜瑋　　　　　　　　　　　　指導教授：三浦篤志 博士

國立交通大學

應用化學系分子科學碩士班

## 摘　　　要

　　奈米粒子特定的排列結構使其可應用在表面科學、微製造技術、生物技術、實驗室晶片以及化學感測原件上。然而奈米粒子的組裝在許多不同的奈米尺度下，至今仍受到許多製造上的限制。因此必須建立出一套新的方法可以控制奈米粒子組裝在特定的位置上。我們的方法其過程包含了(1)藉由連續波雷射聚焦在選定的金奈米粒子上造成局部的溫度上升，(2)熱由金奈米粒子傳至周圍的介質以及懸浮在溶液中的奈米粒子，(3)溫度梯度所引起的對流將溶液中的奈米粒子帶近至金奈米粒子周圍，並形成二維的組裝結構。

　　這篇論文中，我們也探討了不同的奈米粒子的組裝情形。在考慮了上述局部加熱及對流所引起的組裝過程，我們成功地將此方法分別應用在各種不同的奈米粒子溶液中，並形成其他奈米粒子的二維組裝。

　　我們證明並展示雷射能量、照射時間以及溶液中粒子的濃度如何影響組裝的機率和大小。我們的結果明顯地顯示出組裝機率有能量以及粒子濃度的依存性，而組裝大小則有能量及照射時間的依存性。較高的能量提供了

較廣大的加熱區並提高對流的效率，而較高的粒子濃度有助於積聚更多的奈米粒子形成組裝。實驗的結果也支持了我們在局部加熱金奈米使溫度提高上的理論計算，而這部份是根據雷射參數、熱傳導係數及吸收截面的計算。由以上實驗及計算的結果，我們可以藉由操控不同的雷射能量、照射時間及粒子濃度達到控制組裝生成的機制，更可進一步地藉由操控雷射光束在基材上特定的位置產生二維組裝的結構。

# Two-Dimensional Assembly Formation by Temperature Elevation upon Tightly Focused Laser Irradiation on a Single Gold Nanoparticle

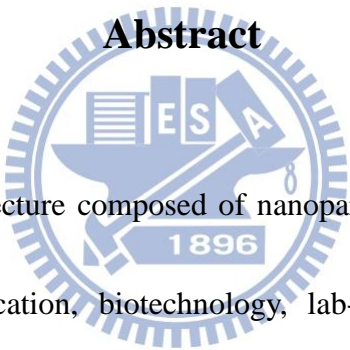**Student: Tzu-Wei Hsu**                    **Advisor: Dr. Atsushi Miura**

**M. S. Program**

**Institute of Molecular Science**

**Department of Applied Chemistry**

**National Chiao Tung University**

## Abstract

Specifically ordered architecture composed of nanoparticles provides applications such as surface science, microfabrication, biotechnology, lab-on-chip, and chemical sensors. However, the methods of assembling nanoparticles in fabricating various nanoscale architectures so far are still limited. Therefore, it is necessary to develop a new method to control the positions and integrations of the nanoparticles in a certain architecture. This study covers the processes of (i) local temperature elevation on a target gold nanoparticle by tightly focused continuous-wave laser illumination, (ii) heat transfer from the gold nanoparticle to surrounding medium and then to suspended nanoparticles in the colloidal solution, and (iii) convection flow induced by gradient of temperature in the solution that bring about the nanoparticles into close vicinity area around the target gold nanoparticle, forming

two-dimensional assembly formation.

In this study, we observed the assembly of different suspended nanoparticles in aqueous solution. By considering the above mentioned processes of the local temperature elevation and convection flow, we have succeeded in developing a new method which can form a two-dimensional assembly formation of various nanoparticles suspended in aqueous solution.

We have demonstrated that how the parameters of continuous-wave laser beam and colloidal solution such as laser power, irradiation time, and particle density affect on the probability and size of the two-dimensional assembly formation. The present results clearly show that the assembly probability depends on laser power and particle density, and the assembly size depends on laser power and irradiation time. A higher laser power provides a wider heated area and enhances convection flow more efficiently, and a higher particle density contributes to accumulate more nanoparticles to form the assembly. This experimental results are supported by our numerical calculations of local temperature elevation on the target gold nanoparticle based on focused laser beam, thermal conductivity, and absorption cross section. Based on overall experimental and numerical results, by varying laser power, irradiation time, and particle density we can control the assembly formation. Further, with this method we can also control the spatial position of the assembly on the substrate by adjustment of the position of the laser beam.

# Acknowledgements

My gratitude goes first and foremost to Prof. Hiroshi Masuhara (Department of Applied Chemistry and Institute of Molecular Science, National Chiao Tung University) for his constant encouragements and guidance of my research works during these two years. His wide knowledge and his logical way of thinking have been of great value for me. His understandings and personal guidance have provided a good basis for the present thesis.

I would extend my heartfelt gratitude to Dr. Takayuki Uwada (Department of Applied Chemistry and Institute of Molecular Science, National Chiao Tung University; currently he moved to Department of Chemistry, Josai University, Saitama, Japan), who led me into the world of research work. Without his patient assists, careful thinking and expert instructions, the completion of this research work would be impossible. I am also greatly indebted to him for his great helps and guidance. Besides, I would like to thank Prof. Kuo-Chu Hwang (Department of Chemistry, National Tsing Hua University), Prof. Hsin-Yun Hsu (Department of Applied Chemistry and Institute of Molecular Science, National Chiao Tung University) for their kindly comments and suggestions, which make this master thesis more complete and fruitful.

I wish to express my special appreciation to Prof. Atsushi Miura, Dr. Anwar Usman, and Dr. Ken-ichi Yuyama (Department of Applied Chemistry and Institute of Molecular Science,

# Table of Contents

# List of Figures

**Chapter 1 Introduction**

**Chapter 2 Theory**

**Chapter 3 Experiment**

**Chapter 4 Two-dimensional Assembly Formation of Various Nanoparticles Suspended in Aqueous Solution**

**Chapter 5 Comparison to Calculation**

# List of Tables

**Chapter 3 Experiment**

# Chapter 1

# Introduction

## 1.1. Micro/Nano structure

In the past two decades, the field of microstructure science and technology can be seen in broad area of worldwide research and application, and such the field has been intensively investigated for a long time and it has been growing explosively. Different from the macrostructure, the size, shape and geometry of microstructure materials were defined in nano- to micro-scale, and the optical and/or properties are different with bulk materials. The science and technique of microstructure fabrication is so-called nanoscience and nanotechnology which have been well known to be able to manipulate the matter on an atomic and molecular scale, and materials may yield interesting properties in a limited micrometer and nanometer-sized environment. Nanotechnology is very diverse in science such as surface science [1, 2], organic chemistry, semiconductor physics, molecule biology [3-5], microfabrication [6, 7], etc. The microstructure nanotechnology already shows an amazing impact quite recently, although nanometer-sized devices and components just begin to apply in medicine [3, 8], biotechnology and lab-on-chip [9, 10], and its huge potential in applications will have a much greater impact in the future.

The scanning tunneling microscopy (STM) and atomic force microscopy (AFM) is the foremost tool for measuring, imaging and manipulating matter at the nanoscale. The STM and AFM can be used to manipulate atoms and nanoparticles, and to assemble them into highly-order architecture on solid surface.
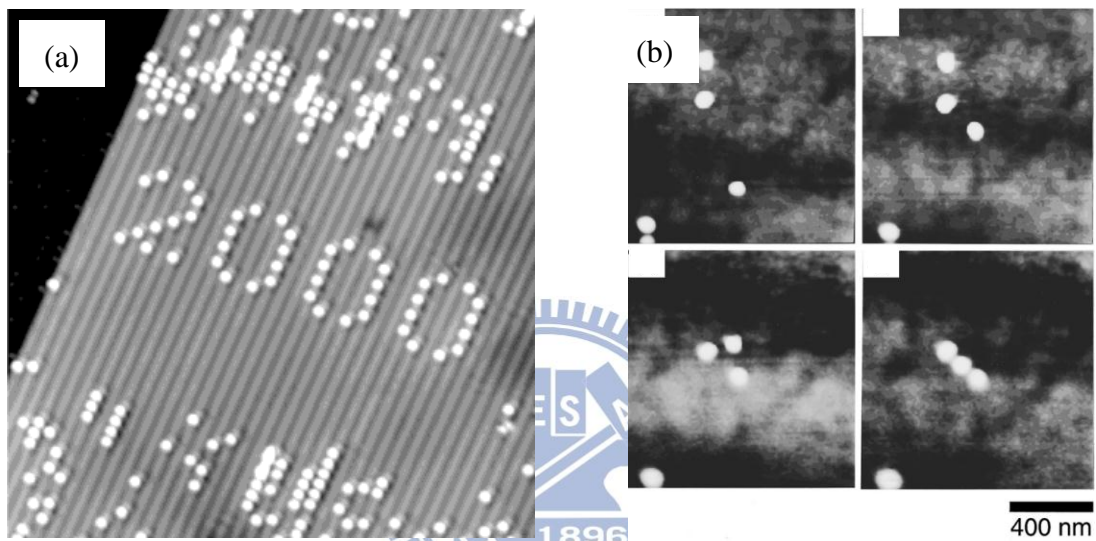


**Fig. 1.1** (a) STM image of CO-molecules as man-made structures by scanning tunneling microscope manipulation [11]. (b) A sequence of AFM images acquired during the formation of a line of GaAs nanoparticles on a GaAs surface. The AFM tip was used to push the particles to their final positions in the line [12].

Top-down and bottom-up are two widely used approaches in nanotechnology for the fabrication of devices or products as schematically shown in Fig. 1.2. Top-down approach looks for forming device in nanoscale by using larger, externally controlled ones to direct their assembly, while bottom-up approach looks for building small device by complex assemblies.

Top-down and bottom-up are two approaches for the nanostructure fabrication, and these approaches are so-called micropatterning techniques. Such as photolithography and inkjet printing has been investigated broadly in top-down approaches [13, 14]. The most common and popular method is photolithography, which has been widely used for miniaturization of structures. For top-down method, it often uses the externally controlled tools to cut, mill, and shape materials to our desire. However, resolution of lithography depends on materials and instruments whose costs increased if miniaturization goes continuously. Thus, a cheaper and simpler method is bottom-up, and self-assembly provides another way to solve and improve the problems which appear in the top-down lithography. Bottom-up method uses the chemical properties of molecule to cause self-organize or self-assemble to form some desired conformations or assemble at specific position. Thus, the bottom-up method is less expensive than top-down one and it also can produce devices in parallel.
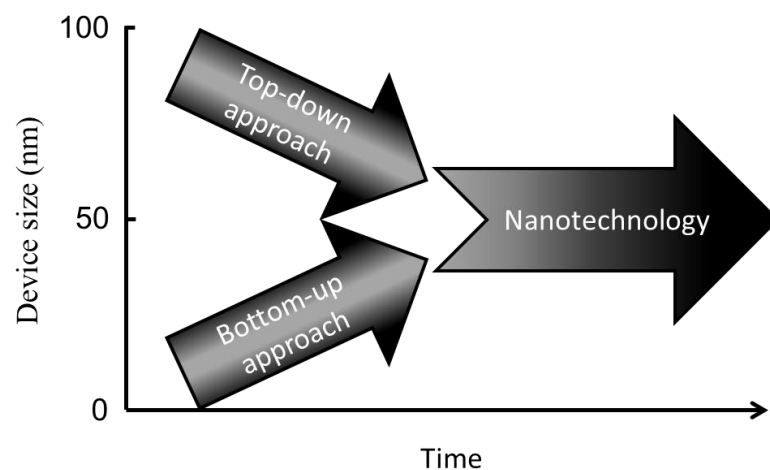


**Fig. 1.2** Nanotechnology is an integration of top-down engineering systems with bottom-up engineering, leading to in a complex, multifunctional, intelligent, and robust system.

## 1.2. Introduction to several two-dimensional assembly methods

Due to the inexpensive progress of bottom-up approach, two-dimensional assembly formation provides another way to construct micro/nanostructure. To assemble functionalized nanoparticles into controlled patterns or architectures yields new useful properties in the fields of electronic, chemical and physical researches, and also provides wide applications in nanoscience and nanotechnology.

Two-dimensional assembly formation of nanoparticles can be applied as micro-lenses in imaging [15] and as masks for evaporation or reactive ion etching to construct periodical arrays of micro/nanostructures [16-18]. In recent years, gold nanoparticle assembled structures have been the most studied mainly due to the fact that it has huge potential applications in broad of fields, for example, electronics, photonics, biological labeling, chemical sensing and imaging, and surface-enhanced Raman spectroscopy (SERS).

For bottom-up method, how to construct a desired nanoparticle assembly and how to establish a procedure become an important target. A number of two-dimensional assembly methods have been previously developed for the arrangement of the nanoparticles on surface in physics, chemistry and biology. Here, we also shortly introduce several two-dimensional assembly methods.

## *1.2.1.  Solvent evaporation*

The interplay between the convectional flow and lateral capillary forces of the particle

plays an important role during the solvent evaporation and its schematic illustration is shown

in Fig. 1.3 [19]. The convection of the nanoparticles from the outer part to the central area,

subsequent sedimentation of the nanoparticles and drying of the solvent provide thin film of

dried solution. At the late step of the drying, the solution height is equivalent to the diameter

of the particles. In that step, convectional flow of the solvent may drag the particles toward

the evaporation center and the capillary forces are exerted upon the nanoparticles due to the

evaporation simultaneously. When the solvent was evaporated, the immobilization of the

nanoparticles on a substrate could be achieved.
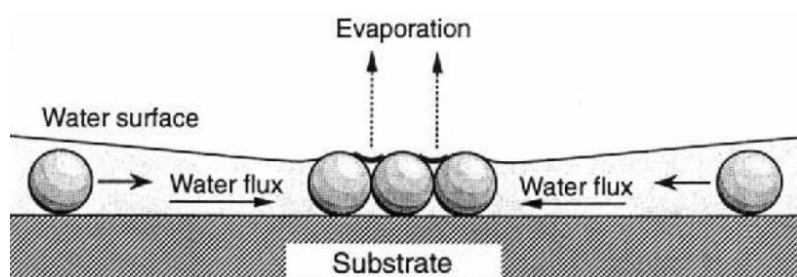


**Fig. 1.3** Schematic presentation of the particle assembly process driven by the liquid flow
[19].
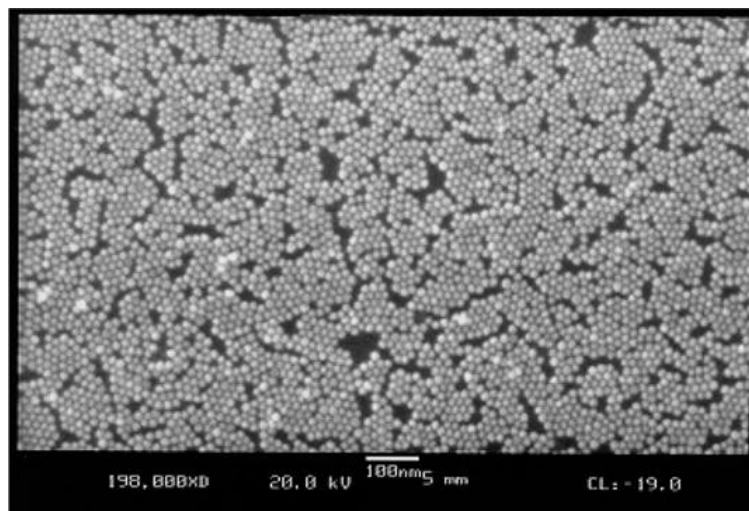
**Fig. 1.4** SEM image of 13 nm gold nanoparticle array on silicon substrate covered with gold nanoparticle aggregate induced by the alcohol methanol solvent evaporation [20].

## *1.2.2. Self-assembled monolayer (SAM)*

Molecular monolayer formation has been studied systematically from the 19th century. In the earlier studies, the structure and processes on the molecular level could not be manipulated due to the lack of appropriate tools. The understanding on a microscopic level of SAM and its progress started in the 1980s. With the microscopic tools available today, the substrate surface modification of SAM layer has been applied to organics and patterned surfaces, and it also plays an important role in bio-technological devices.

SAMs are properly organized structure of amphiphilic molecules, and they are grown from solution or from the gas-phase. All the molecules in the SAMs have a head group end

with a specific affinity to the substrate and on the other end is called tail group with a

functional group terminal as shown in Fig. 1.5. By using various kinds of molecules with

different substrates, one can construct SAMs for various applications.
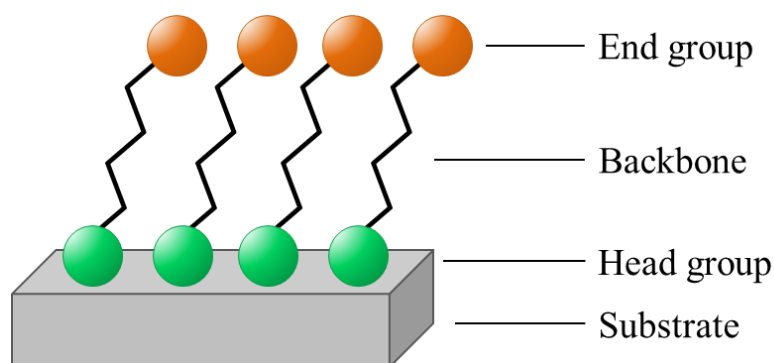


**Fig. 1.5** Schematic picture of a self-assembled monolayers (SAMs) structure.

SAMs can be constructed by the chemisorption of head group of substrate in both liquid

and vaporization condition. Molecules are adsorbed into the lower surface energy layer

readily due to the strong chemisorption of the head groups. The head groups assemble till no

area to grow on the surface, and it forms the totally covered and packed single SAM.

Nanoparticles can be deposited onto SAM surface by cross-linking approach via specific

terminal group absorption. Thus we can produce SAM surface homogenously covered with

two-dimensional assembly of nanoparticles (Fig. 1.6, Fig. 1.7).
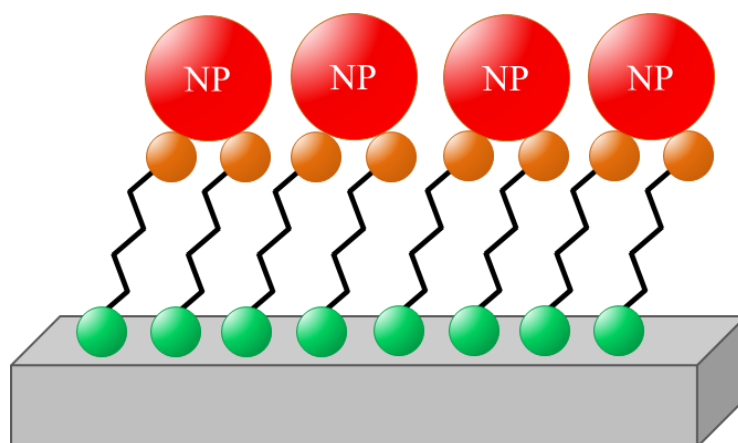
**Fig. 1.6** Schematic picture of nanoparticles immobilizing on terminated self-assembled monolayers (SAMs) of organic molecules.
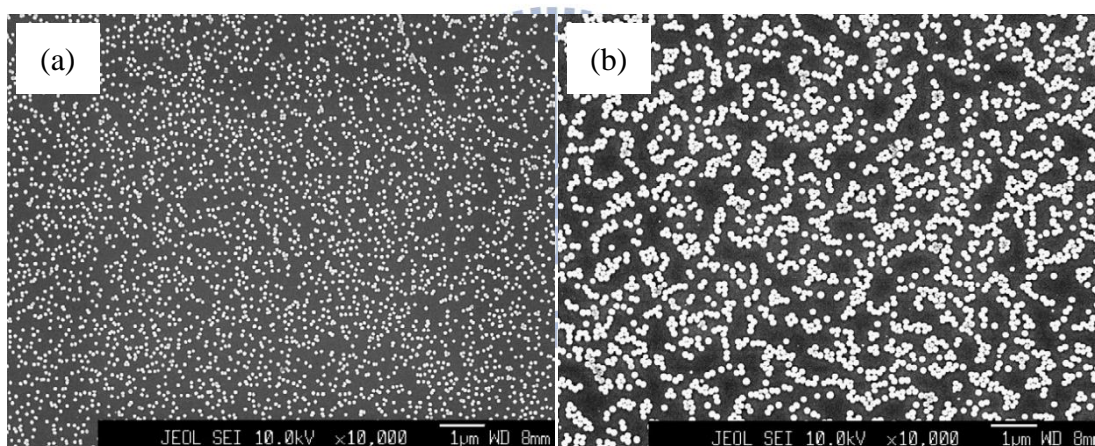


**Fig. 1.7** (a) SEM images of a 3-MPTS coated silica wafer surface after dipping in a gold nanoparticle suspension for 1h and (b) a 3-MPTS coated gold surface after dipping in a silica nanoparticle suspension for 1h [21].

## 1.2.3. *Optical tweezers*

Ashkin and co-workers [22-25] demonstrated that micrometer-sized objects such as microbeads, microspheres, and biological cell can be trapped and manipulated at focus spot using optical tweezers. Now the size of trapped object has been reduced from micrometer to nanometer, and studies on optical traps continue to find applications in physics, chemistry and biology.

Optical trap can be formed by a tightly focusing laser beam with a high numerical aperture objective lens. The force on a micro particle can be decomposed into two components; one is a gradient force in the direction of the spatial light gradient and another one is a scattering force in the direction of the light propagation. To form a stable trap, the light must be focused, producing a tree-dimensional intensity gradient. Two representative lights are again refracted by the bead but the change in momentum in this instance leads to a net force towards the focus, which the schematic presentation was shown in Fig. 1.5 [26].
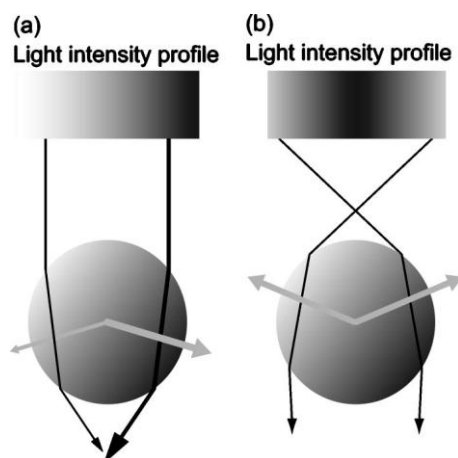


**Fig. 1.8** Gray arrows represent the force. (a) The bead is illuminated by a defocus beam of light with a radial intensity gradient. (b) A focus beam illuminates on the bead [26].

9

The lateral forces balance each other and the axial force is balanced by the scattering force, which decreases away from the focus. If the bead moves in the focused beam, the imbalance of optical forces will draw it back to the equilibrium position.

It can trap a particle easily by balancing these two force contributions and the particle can be dragged inside the solution by moving the focus spot of laser beam with a speed less than the critical speed which determines the viscous force due to the surrounding aqueous medium. After capturing the particle from the solution, we can drag them toward the position where we wanted. Eventually, we can overcome the electrostatic repulsion between one object to another object and fix them by utilizing an adhesive electrostatic force between object and substrate. By repeating this steps several times, it can demonstrate the specific two-dimensional structure [27] as shown in Fig. 1.9.
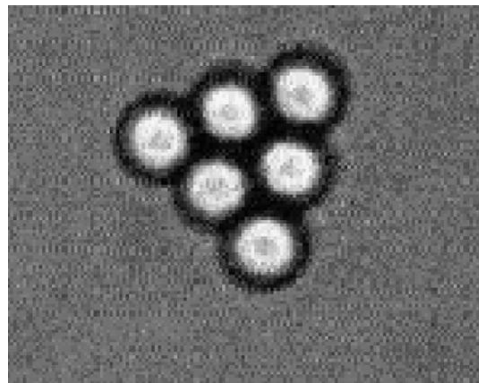


**Fig. 1.9** Planar arrangement of silica spheres [27].

## 1.3. Assembly of nanoparticles by laser-formed micronanobubble

S. Fujii, et al [28-31] demonstrated ring structure formation of nanoparticles by a laser-induced micronanobubble on a gold thin film. The ring-shaped structures in micro- or nano-scale have a novel potential for application in optical and electronic resonators, magnetic storage, sensors and spintronic devices, and this laser-induced micronanobubble technique also can be applied in manipulating sequential single DNA strands [29] and crystallization [31].

Thus, laser irradiation upon a gold thin film causes temperature elevation and leads to micronanobubble formation. Due to the specific optical property of this gold thin film which consists of gold nanoparticles is different with bulk gold and the high absorption coefficient at 1064 nm of gold nanoparticle is caused by localized plasmon resonance and results in local heating up to the boiling temperature of water. Continuous-wave laser-induced local heating generates bubbles on gold thin film surface and it also causes a temperature gradient, which leads to a surface tension ($\gamma$) gradient vertical to the bubble and its schematic illustration is shown in Fig. 1.10 (b).
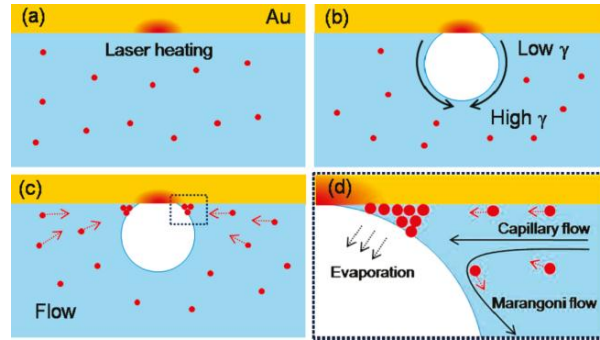
**Fig. 1.10** Schematic illustration of the assembly mechanism of quantum dots (red dots) based on micronanobubble formation and fluidic flow [30].

The surface tension decreased with temperature increasing leads to surface tension gradient from the nearest side of the gold surface (low $\gamma$) to the further side (high $\gamma$) along the bubble interface and induces fluidic flow convection, namely, Marangoni convection. Nanoparticles dispersed in water are drawn toward the focal point and assembled at the interface between the bubble and gold surface via induced fluidic flow by Marangoni convection. Not only Marangoni convection but also capillary flow is induced by phase transition of water from liquid to gas as shown in Fig. 1.10 (d). Thus, the nanoparticles are agglomerated at the stagnation point made by the Marangoni flow and evaporation-induced capillary flow. The FE-SEM image of the ring shape of quantum dots assembled is shown in Fig. 1.11.
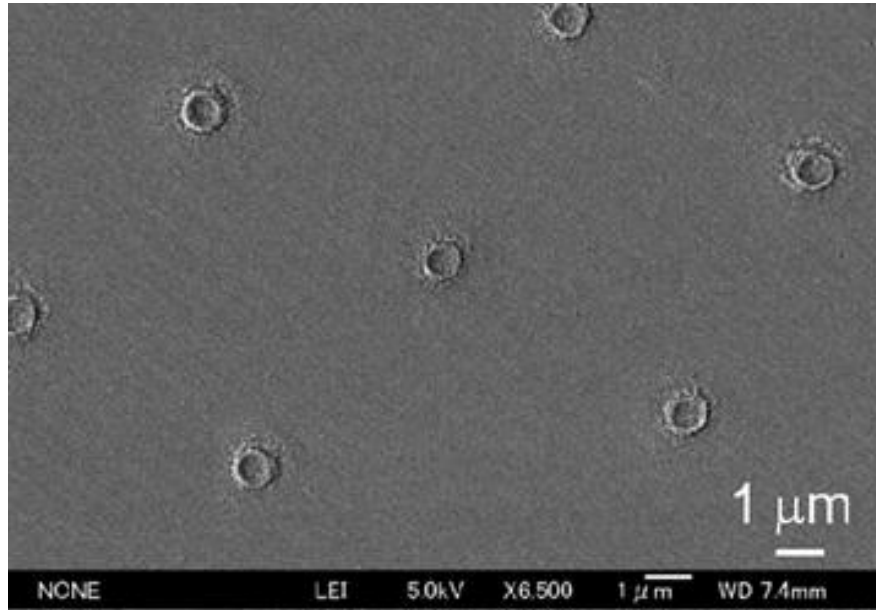
**Fig. 1.11** FE-SEM image of the quantum dots ring array on a gold surface.
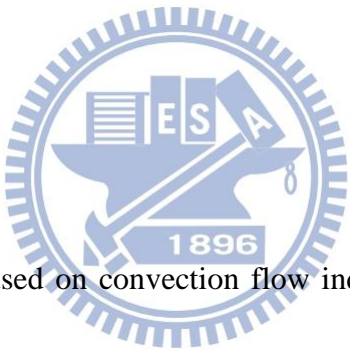
## 1.4. Laser-heating induced nanostructure formation

A number of two-dimensional assembly methods have been developed in view of the immobilization of nanoparticles on surface. However, these methods typically take long time or limited materials of nanoparticle and substrate. Some of them usually involve multiple and complicated steps for the patterning of the substrate surface. In this study, we present a simple method for nanoparticles assembled in two-dimension.

Upon continuous-wave laser illumination, higher absorption coefficient of gold nanoparticle causes an easy local temperature elevation. A laser-illuminated particle absorbs the irradiated laser energy causing its temperature high, and acts as a point heat source on the surface of the substrate [32]. The temperature of gold nanoparticle enhances in nanosecond

during trapping laser irradiation. The heat energy transfer takes place from the gold nanoparticle to solution subsequently. The heat transfer cause temperature gradient and it induces convection flow, resulting in mass transfer toward the heated source. The nanoparticles in the solution can be fixed on substrate through electrostatic force between nanoparticles and substrate. The nanoparticles were adhered strongly on the substrate after removing the solution, and the obtained result indicates that the binding of the nanoparticles to substrate is quite stable. Finally, we can form two-dimensional assembly by coupling the laser heating and convection flow.

## 1.5. Aim

In this work, we have focused on convection flow induced assembling of nanoparticle upon laser irradiation and tried to clarify how laser power, irradiation time, and particle density of nanoparticle aqueous solution determine on the two-dimensional assembly probability and the size of assembly. We also tried to use various nanomaterials from polymer and semiconductor to metallic nanoparticle for further applications of the assembly formation. To confirm a mechanism and to establish an easier method of the two-dimensional assembly formation clearly are our expectations.

# Chapter 2

# Theory

## 2.1. Optical property of gold nanoparticle

In the past few decades, humans rely on electronic devices to new heights of human civilization and, from the beginning of the vacuum tubes, the size of electronic products continue to shift to a smaller size. However, the development of modern electronic components gradually encountered obstacles of size problem and then narrowing the size leads to decreased bandwidth. Although the photonic components provided a larger bandwidth than electronic components, but its size was confined by diffraction limit. The surface plasmon provides good convergence of electronic and photonic components, and bridging the two components can be integrated in one of the advantages and hot topics.

Surface plasmon resonance is a collective oscillation of the electrons that may exist at the interface of two media with dielectric constants of opposite signs, for instance, a metal and a dielectric. In early 20$^{th}$ century, the irregular diffraction spectrum from metallic gratings due to the excitation of surface plasma waves was first described by Wood [33]. Gustav Mie pointed out firstly that the interaction of incident light with metallic nanoparticles results in the collective oscillation, and presented a solution to Maxwell's equation [34] that describes

the extinction spectra of spherical particles of arbitrary size. The large enhancement of the

local surface electric field on the metallic nanoparticles surface leads to a strong enhancement

of the spectroscopic signal from molecules around the nanoparticles [35]. This effect is

so-called surface-enhanced Raman scattering (SERS) [36-38].

Apart from the surface plasmon resonance that can be induced on metal surface, plasmon

resonance also can be induced on small metallic spherical particle. The free electrons in the

metal (d electrons in gold) are free to move through the material. When wavelength of light is

much larger than the nanoparticle size, the oscillating electric field induces the free electrons

in the metal to oscillate coherently. As the wave of the light passes through the nanoparticle,

the electron density in the nanoparticle is polarized on surface and oscillates in resonance with

the frequency of light. The collective oscillation of the elections is called the dipole plasmon

particle resonance and the schematic picture is shown in Fig. 2.1 [39].
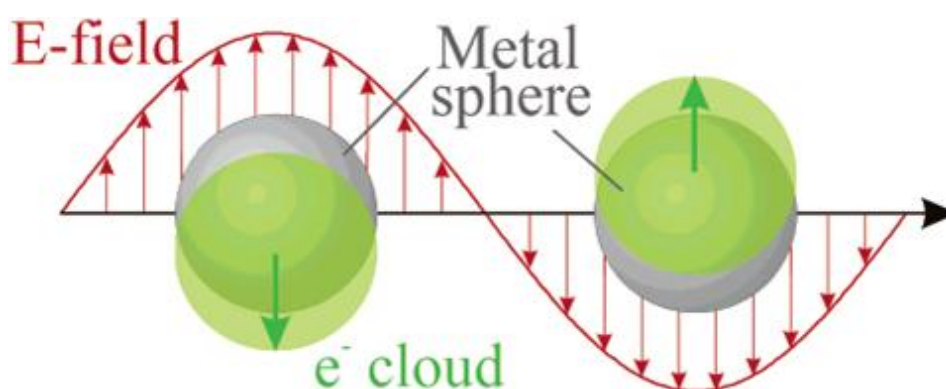


**Fig. 2.1** Schematic of plasmon oscillation for a sphere, showing the displacement of the
conduction electron charge cloud relative to the nuclei [39].

The resonance frequency is determined from adsorption and scattering spectroscopy, and it is found to be relative to the size, shape, and dielectric constants of both the metal and the surrounding material. As the size and shape of the nanoparticle change, the surface geometry is changed and it causes the electric density shift on the surface. This causes the resonance frequency change and makes a different cross-section for the optical properties such as absorption and scattering. Due to the different ability of the surface to accommodate electron density from the nanoparticle, changing the surrounding material causes dielectric constant modification and affects on the resonance frequency.

Because of the spherical nanoparticle is much smaller than wavelength of light we can consider that the electric field of the light can be treated as constant. Thus we can use the quasi-static approximation to describe the collective oscillation of electrons. We consider that a very small spherical metal nanoparticle (radius $= a$) is suffered from an electric field by the vector $\vec{E}$. We take this constant vector to be in the $z$ direction, $\vec{E} = E_0\hat{z}$, where $\hat{z}$ is an unit vector. The dielectric constant of the metal nanoparticle is $\varepsilon_n$, and the dielectric constant of the surrounding medium is $\varepsilon_m$. The schematic figure of that spherical metal nanoparticle under electric field is shown in Fig. 2.2.
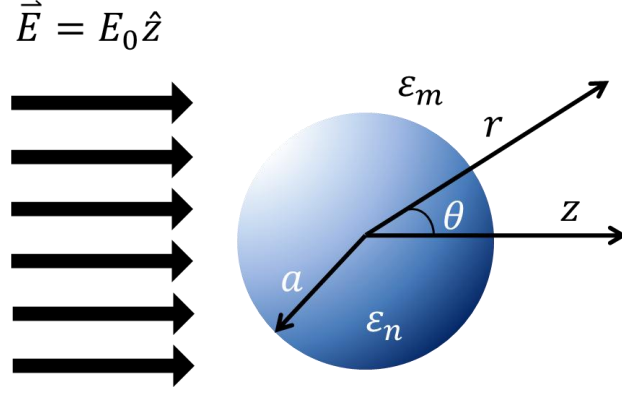
**Fig. 2.2** A metallic nanoparticle, which radius and dielectric constant are $a$ and $\varepsilon_n$, respectively, situated in a homogenous electric field $\vec{E} = E_0\hat{z}$. Dielectric constant of surrounding medium is $\varepsilon_m$.

Under the constant amplitude of illumination, the polarizability is related with refractive index

of gold nanoparticle and given by

$$\alpha_o = \left(3V\frac{\varepsilon_n-\varepsilon_m}{\varepsilon_n+2\varepsilon_m}\right), \tag{Eq. 1}$$

Due to the scattering and absorption of nanoparticle, the polarizability was made to include

the radiative reaction, which attenuates the incident field giving complex polarizability

$\alpha = \alpha_1 + i\alpha_2$ as

$$\alpha = \left(3V\frac{\varepsilon_n-\varepsilon_m}{\varepsilon_n+2\varepsilon_m}\right) + i\left(\left|\left(3V\frac{\varepsilon_n-\varepsilon_m}{\varepsilon_n+2\varepsilon_m}\right)\right|^2 \frac{k^3}{6\pi\varepsilon_m}\right), \tag{Eq. 2}$$

where $V$ is the volume of gold nanoparticle. The real part in Eq. 2 corresponds to the

scattering of light while the imaginary part affects the absorption. For larger metallic

nanoparticles, their collective behavior modifies overall dielectric property of system. Due to

finite penetration-depth ($\delta$), the volume ($V \propto a^3$) of large metallic nanoparticle should be

modified with effective volume as

$$V' = 4\pi \int_0^a r^2 \exp[(r-a)/\delta]\,dr = 4\pi\{a^2\delta - 2a\delta^2 + 2\delta^3(1-\exp(-a/\delta))\}, \text{(Eq. 3)}$$

where $r$ is the fraction of particle volume uniformly polarized. Therefore, the gradient force

is given by

$$F_{grad} = \frac{3}{2}\left|\frac{\varepsilon_n - \varepsilon_m}{\varepsilon_n + 2\varepsilon_m}\right|\nabla\langle E^2\rangle V', \qquad\qquad \text{(Eq. 4)}$$

where $\varepsilon_n(\lambda) = \varepsilon_1(\lambda) + i\varepsilon_2(\lambda)$ and $\varepsilon_m = n_m^2$. Complex dielectric constant $\varepsilon_n(\lambda)$ relates

with $n(\lambda)$ as $\varepsilon(\lambda) = n^2(\lambda)$ giving $\varepsilon_1 = n_1^2 + n_2^2$ and $\varepsilon_2 = 2n_1 n_2$. Therefore, the gradient,

scattering, and absorption force is given as

$$F_{scat} = \frac{n_m\langle S\rangle C_{scat}}{c}, \qquad\qquad \text{(Eq. 5)}$$

$$F_{abs} = \frac{n_m\langle S\rangle C_{abs}}{c}, \qquad\qquad \text{(Eq. 6)}$$

$$F_{grad} = \frac{1}{2}|\alpha|\nabla\langle E^2\rangle, \qquad\qquad \text{(Eq. 7)}$$

and scattering and absorption cross sections of the metallic nanoparticle is given by

$$C_{scat} = \frac{k^4|\alpha|^2}{4\pi}, \qquad\qquad \text{(Eq. 8)}$$

$$C_{abs} = k\mathrm{I}_m(\alpha), \qquad\qquad \text{(Eq. 9)}$$

where $k = 2\pi n_m/\lambda$ is the wavenumber in water, $\langle S\rangle$ is the time averaged Poynting vector

of electromagnetic wave, and $n_m$ is refractive index of water. The metallic nanoparticle

scattering and absorption cross section is the ratio to efficiency with the geometrical

cross-section $\pi a^2$ and given by

$$Q_{scat} = \frac{C_{scat}}{\pi a^2}, \qquad\qquad \text{(Eq. 10)}$$

$$Q_{abs} = \frac{C_{abs}}{\pi a^2},$$ (Eq. 11)

and the extinction efficiency is $Q_{ext} = Q_{scat} + Q_{abs}$. The relative calculation will be evaluated and discussed in Chapter 5 in detail.

## 2.2. Photo-thermal effect on optical property of gold nanoparticle

Upon optical illumination, metal nanoparticles can absorb energy from electromagnetic field of light and subsequently generate heat efficiently. Thus, according to the useful thermal property, metal nanoparticles can be targeted as thermal agents and be applied usefully in medical therapies and biotechnology. The efficient temperature elevation is due to that a strong resonance occurs at the electromagnetic frequency $\omega_{SPR}$ where $\varepsilon_m = -2\varepsilon$. This surface plasmon resonance causes large local electric field enhancement and enhances light absorption and scattering by the nanoparticle at the surface plasmon resonance frequency $(\omega_{SPR})$.

The intensity distribution of incident light near the focal point will be of the form

$$I_{xy} = I_0 \left\{ \frac{\frac{2\pi}{\lambda} J_1(NA \cdot r)}{\frac{2\pi}{\lambda} NA \cdot r} \right\}^2,$$ (Eq. 12)

where $I_0$ is the maximum intensity of the pattern at the Airy disc center (x = y = 0), $\lambda$ is the wavelength, $NA$ is the numerical number, and $J_1$ is the Bessel function of first order. The intensity at the center of the focus will be

$$I_0 = P \cdot \pi \frac{NA^2}{\lambda^2}, \tag{Eq. 13}$$

where $P$ is the total power of the laser beam, and the relation between instantaneous incident power $P$ and $I_0$ is obtained from energy conservation. Based on result by Keblinski et al. [40], the temperature changed with irradiation time and distance from the heated nanoparticle center is given by

$$T(r,t) - T_\infty = \frac{\left(\frac{dQ}{dt}\right)}{4\pi r k}\left\{erfc\left(\frac{r-r_p}{2\sqrt{Dt}}\right) - exp\left(\frac{r-r_p}{r_p} + \frac{Dt}{r_p}\right)erfc\left(\frac{r-r_p}{2\sqrt{Dt}} + \frac{\sqrt{Dt}}{r_p}\right)\right\}, \tag{Eq. 14}$$

where $T_\infty$ is the temperature far away from the nanoparticle, $dQ/dt$ is the total power absorbed by nanoparticle, and $r$ is the distance from the particle center. In addition, erfc is the complementary error function, $r_p$ is the nanoparticle radius, $k$ is the heat conductivity of surrounding medium, $D$ is the thermal diffusivity of the medium, $D = k/\rho c_p$, where $\rho$ is the density and $c_p$ is the specific heat. To solve the Eq. 14, the initial temperature correspond to heating starting at time, $t = 0$, can be given by

$$T_{in}(r,t) = T_\infty, \tag{Eq. 15}$$

where $T_\infty$ is room temperature here. Thus, under steady state conditions, the radial temperature around nanoparticle is

$$T = T_\infty + \frac{\left(\frac{dQ}{dt}\right)}{4\pi r k}, \tag{Eq. 16}$$

the total power absorbed of nanoparticle, $dQ/dt$, corresponds to absorption cross section and light intensity, $C_{abs}$ and $I_0$, respectively, and given by

$$\frac{dQ}{dt} = C_{abs} \cdot I_0 = C_{abs} \cdot P \cdot \pi \frac{NA^2}{\lambda^2}, \tag{Eq. 17}$$

We demonstrate a model of that the gold nanoparticle absorbs laser light and temperature enhancement resulting in heat transfer into the surrounding medium. The radial temperature-change profiles from gold nanoparticle surface to surrounding will be calculated and discussed in Chapter 5 in detail.
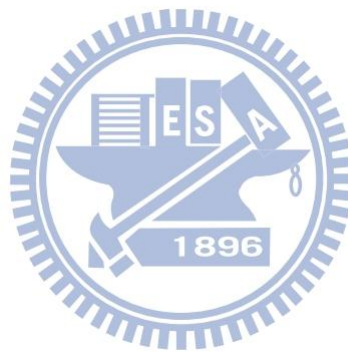
# Chapter 3

# Experiment

## 3.1. Experiment setup

### *3.1.1. Continuous-wave laser light source*

Laser is a device that emits light through a series process of optical amplification based on the stimulated emission of photons in the optical cavity. The optical cavity, resonator normally consists of two mirrors between which a coherent beam of light travel in both directions. Photon will pass through the gain medium repeatedly by reflecting it onto the two mirrors. When the amplification in the medium is larger than loss in the resonator, then the power of the light can be enhanced exponentially. Continuous-wave (CW) operation of a laser means that the laser is pumped and emits light continuously. The balance of pump power against gain saturation and cavity losses produces an equilibrium value of the laser power inside the optical cavity. It means that the continuous-wave operation requires the population inversion of the gain medium to be continually refilled by a stable pump source and the output power is constant over long time periods.

A continuous-wave laser can be achieved by using atoms that has two relatively stable levels between their ground state and excited state, which is called four-level laser. In this

system, the pumping transition excites the atoms in the ground state into the excited state. From excited state, the atoms decay by a fast, non-radiative transition into the higher metastable state. Since the lifetime of the laser emission is long compared to that of non-radiative transition, a population accumulates in higher metastable state, which may relax by spontaneous or stimulated emission into lower metastable state. And the lower metastable state likewise has a fast, non-radiative decay into the ground state. As before, the fast and radiationless decay transitions results in population of the excited state and lower metastable state being quickly depleted. Since any appreciable population accumulating in higher metastable state will form a population inversion with respect to lower metastable state, thereby maintaining the population inversionis needed for continuous-wave laser operation.
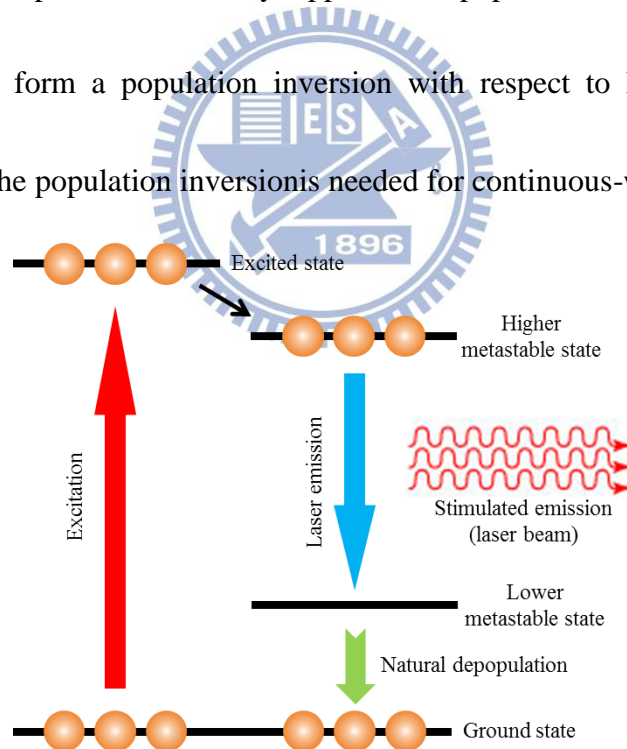


**Fig. 3.1** A four-level laser energy diagram.

In our study, we used CW Nd:YVO$_4$ laser (Spectra Physics; BL-106C,wavelength; 1064 nm) as the laser source. There are several kinds of vanadate laser is usually used based on

neodymium doped vanadate crystals such as yttrium vanadate (Nd:YVO$_4$), gadolinium vanadate (Nd:GdVO$_4$), lutetium vanadate (Nd:LuVO$_4$), and yttrium aluminum garnet (Nd:YAG). The high absorption coefficient, cross section, broad gain bandwidth, broad wavelength region for pumping and short upper state lifetime of vanadate make it useful for the high power generation, and it leads to high heat conductivity of the doped materials. The typical laser emission wavelength for Nd:YVO$_4$ is 1064-nm and it is always diode-pumped.



**Fig. 3.2** A picture of continuous-wave Nd:YVO$_4$ laser.

## 3.1.2. Confocal microspectroscopic system

Confocal microspectroscopic measurement was carried out to obtain scattering spectrum and fluorescence image with the confocal unit (Olympus; FV300) coupled optical inverted microscope (Fig. 3.3). The scattered light from a single gold nanoparticle was collected with an objective lens through a pair of scanning galvano mirrors in the confocal unit and the spectrum was recorded by a CCD camera (Princeton; PIXIS 400) couple with polychromator (Princeton; SpectraPro 2300i).

Fluorescence images were obtained by exposing 488-nm Ar-ion laser beam through a line filter and an objective lens (Olympus; ×60, N.A.: 0.9) to the sample placed on the microscope stage and were recorded by a CCD camera coupled with polychromator.
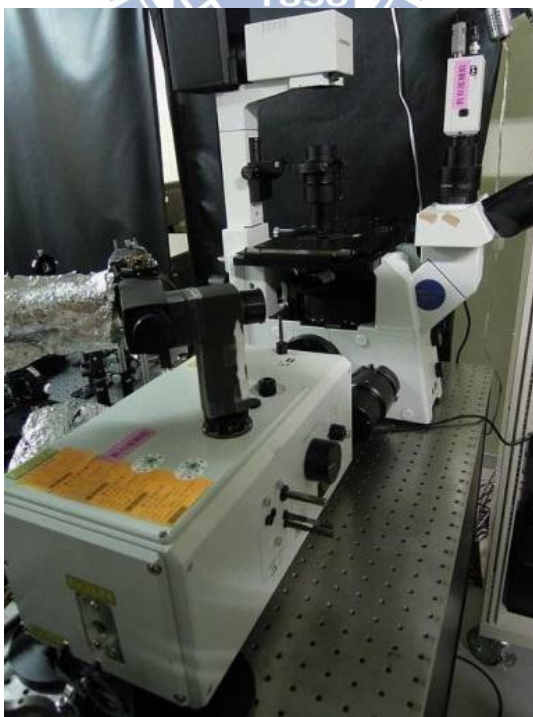


**Fig. 3.3** A picture of confocal microspectroscopic system.
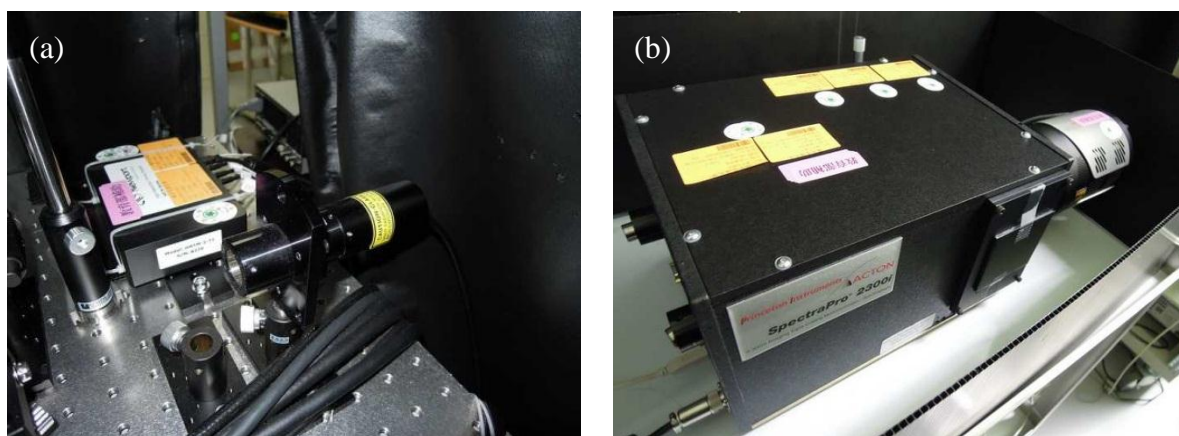
**Fig. 3.4** Pictures of (a) 488-nm Ar-ion laser and (b) CCD coupled with polychromator, respectively.

## *3.1.3. Experiment setup*

The experimental setup is shown in Fig. 3.5. The continuous-wave Nd:YVO$_4$ laser was introduced to an inverted microscope (Olympus; IX-71) through objective lens (Olympus; × 60, N.A.: 0.9). The focal area and beam waist are $3.8\times10^{-9}$ cm$^2$ and about 700 nm, respectively. The laser power was adjusted by using a polarizing beam splitter and was measured after the objective lens by a power meter (Spectra Physics; 842-PE). The sample was placed on an inverted microscope, and it was illuminated with a white light from a 100 W halogen lamp through an oil-immersion dark-field condenser (Olympus; U-DCW, N.A.: 1.2-1.4). The dark field image was observed with a digital CCD camera (JAI; CV-S3200) attached to the microscope and prepared assembly were examined by SEM (JEOL JSM-7401F). All the experiments were carried out at room temperature (20℃).
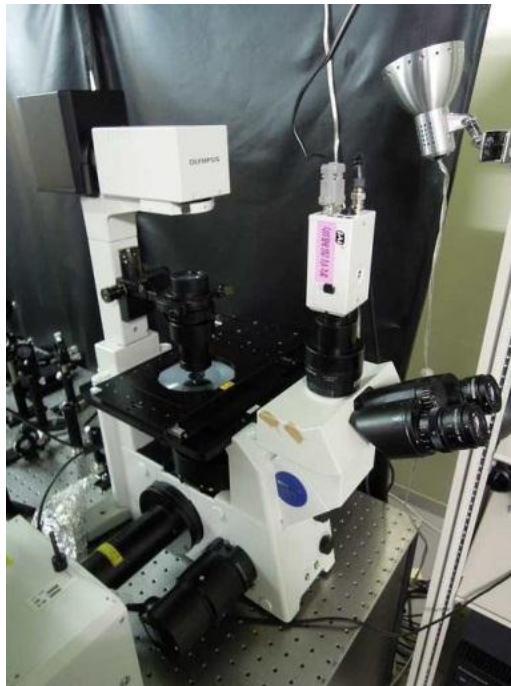
**Fig. 3.5** A picture of inverted microscope.
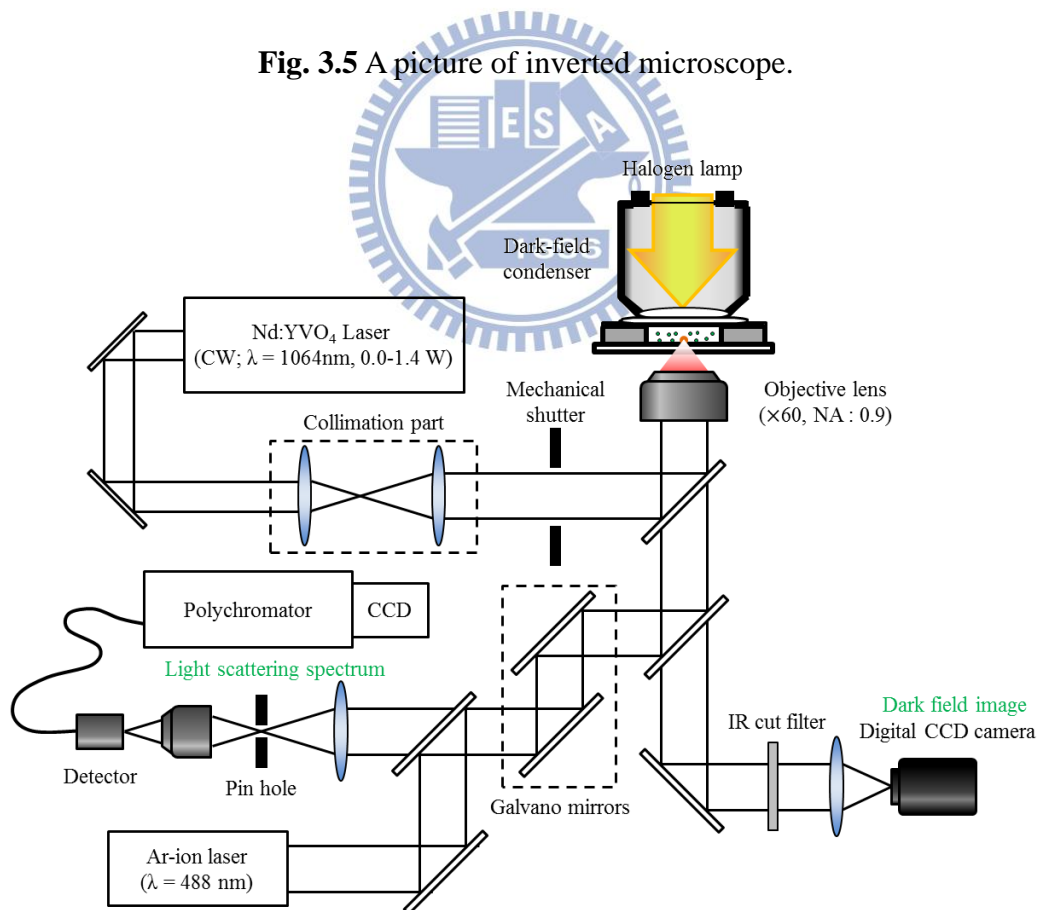


**Fig. 3.6** An illustration of experimental setup.

## 3.2. Sample preparation

Mother gold nanoparticles (BBInternational; EM.GC200, mean diameter: 200 nm) were

dispersed and fixed on the glass substrate by spin coating. The glass substrate was already

cleaned by a plasma cleaner (ATTO; diener electronic) before spin coating. The prepared

sample substrate was covered with a CoverWell perfusion chamber (Grace Bio-Labs; depth:

1.0 mm, diameter: 20 mm), and the chamber was filled with various nanoparticles suspended

in aqueous solution which is mentioned below.
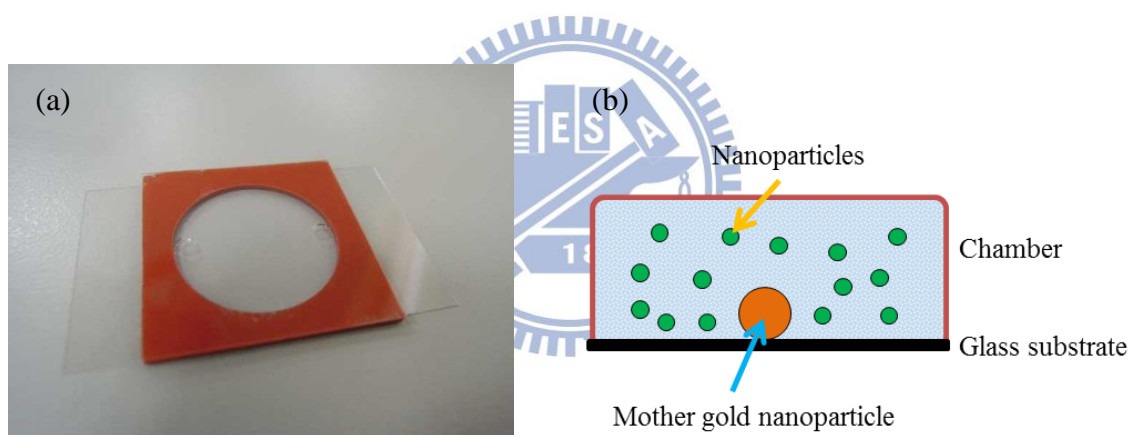


**Fig. 3.7** (a) A picture of nanoparticles suspended in aqueous solution covered with perfusion
chamber. (b) A schematic diagram of nanoparticles aqueous solution covered with perfusion
chamber.

Fluorescent polystyrene beads solution (diameter: 50 nm, density: 1.055 g/cm$^3$, ex/em:

529 nm/546 nm) was purchased from PolyScience. It was diluted to the particle density of

roughly $3.9 \times 10^{13}$, $3.9 \times 10^{12}$, $3.9 \times 10^{11}$, $3.9 \times 10^{10}$ and $3.9 \times 10^{9}$ particles/mL by deionized

water, respectively. Quantum dots solution (Qdot® 585 ITK™ carboxyl quantum dots, diameter: 20 nm) was purchased from Invitrogen. It was diluted to the concentration 8 nM by deionized water. Gold nanoparticles solution (EM.GC100, mean diameter: 100 nm) was purchased from BBInternational. It was diluted to the particle density about $5.6 \times 10^6$ particles/mL by deionized water. Poly(*N*-isopropylacrylamide) molecule solution was prepared with deionized water, and its concentration were 200 mg/mL and 500 mg/mL, respectively.
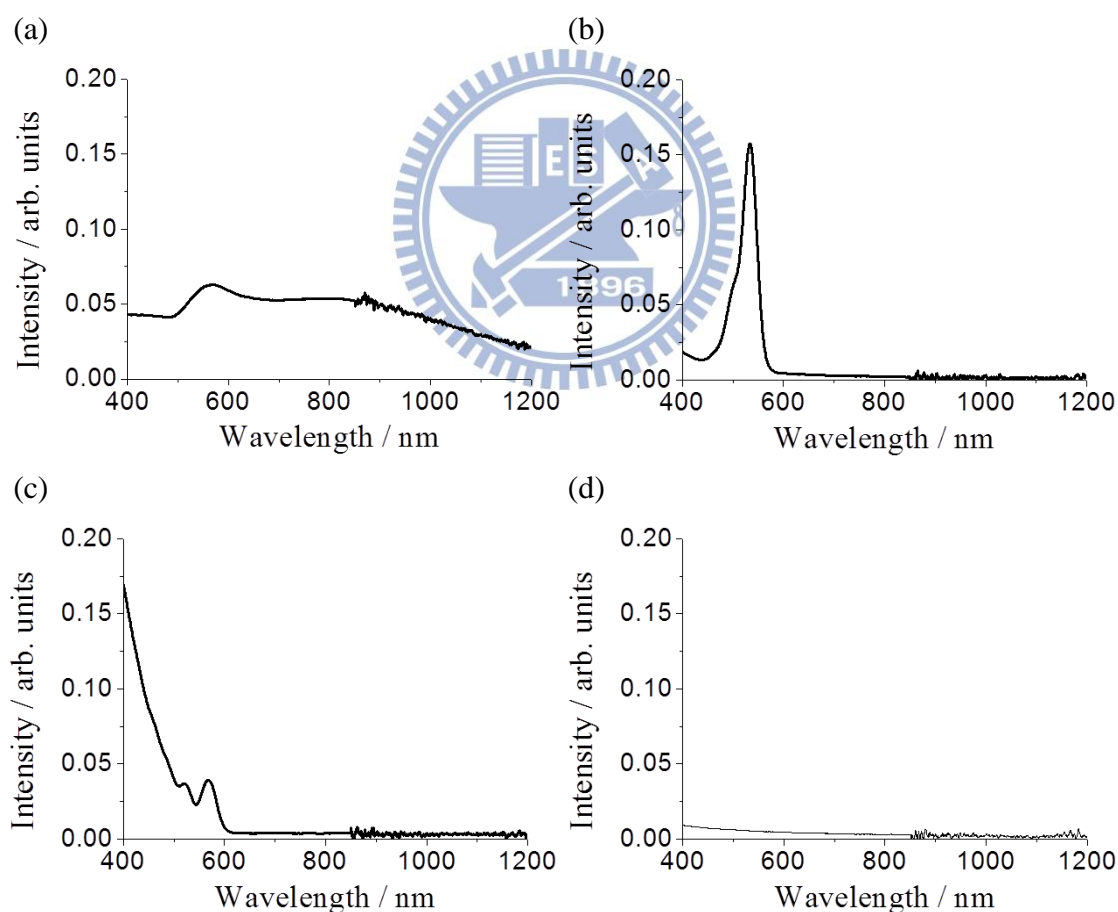


**Fig. 3.8** Absorption spectra of (a) 200 nm gold nanoparticles, (b) 50 nm fluorescent polystyrene beads, (c) 20 nm quantum dots, and (d) PNIPAM molecules suspended in aqueous solution, respectively.

## 3.3. Thermal properties of the suspended nanoparticles

The thermal property of materials which we used is shown in Table 3.1 and Table 3.2.

**Table 3.1**

|  | Size (nm) | Heat conductivity (W/m · K) | Specific heat capacity (J/Kg · K) |
|---|---|---|---|
| Polymer nanoparticle (Polystyrene) | 50 | 0.12 [41] | 1219 [41] |
| Quantum dot nanoparticle (CdSe) | 20 | 9 [42, 43] | 250 [43, 44] |
| Gold nanoparticle | 100 | 317 [45] | 129 [45] |
| Water | - | 0.616 [45] | 4200 [45] |
| Glass substrate | - | 1.125 [46] | 720 [47] |

**Table 3.2**

|  | Average molecule weight | Phase transition temperature (℃) |
|---|---|---|
| Poly(N-isopropylacrylamide) (PNIPAM) | 10205 | 32 |

# Chapter 4

# Two-dimensional Assembly Formation of Various

# Nanoparticles Suspended in Aqueous Solution

## 4.1. Introduction

Based on the numerical prediction in Chapter 2, we know that the temperature of gold nanoparticle is elevated by laser irradiation due to large adsorption cross section, as given by the calculation using Mie theory. Such the temperature elevation of a single gold nanoparticle (we called this single gold nanoparticle as "mother gold nanoparticle") attracts the nanoparticles suspended in the solution to the mother gold nanoparticle via convection flow, which is induced by the temperature gradient. We found that the gathered nanoparticles form a two-dimensional assembly. In this study, we employed 1064-nm CW laser tightly focused on the mother gold nanoparticle (d: 200 nm) in the presence of a various kind of nanoparticles suspended in aqueous solution. Dark-field microscopy was utilized to observe the scattering light around the mother gold nanoparticle.

## 4.2. Two-dimensional assembly formation of fluorescent polystyrene beads

Fluorescent polystyrene beads (with excitation wavelength at 488 nm) are used as suspended nanoparticles. We observed that the scattering light intensity increased when the mother gold nanoparticle is irradiated, as shown by a series of images in Fig. 4.1. Importantly, the scattering light intensity after irradiation is higher than that before irradiation. To confirm such scattering light intensity change, we evaluate the fluorescence image around the mother gold nanoparticle by using confocal microscopic imaging and SEM, as shown in Fig. 4.2 and Fig. 4.3, respectively. As the result, they clearly show that there is a doughnut-shaped two-dimensional assembly formation of the fluorescent polystyrene beads around the mother gold nanoparticle. The assembly formation is also supported by the line profile of the fluorescence image, where the fluorescence intensity around the center is extremely higher than surrounding area (Fig. 4.2 (b)). The local minimum of fluorescence intensity at the center indicates that there are no polystyrene beads on the top of the mother gold nanoparticle. Based on this finding, we interpret that during laser irradiation there are a large number of polystyrene beads gathered around the mother gold nanoparticle by either gradient force due to optical trapping phenomenon or convection flow related to laser heating. The temporary gathered polystyrene beads are not entirely formed into an assembly, and thus they partially are dispersed into the surrounding area when the trapping laser is switched off. Therefore, we

only observed two-dimensional assembly formation attached on the glass substrate.
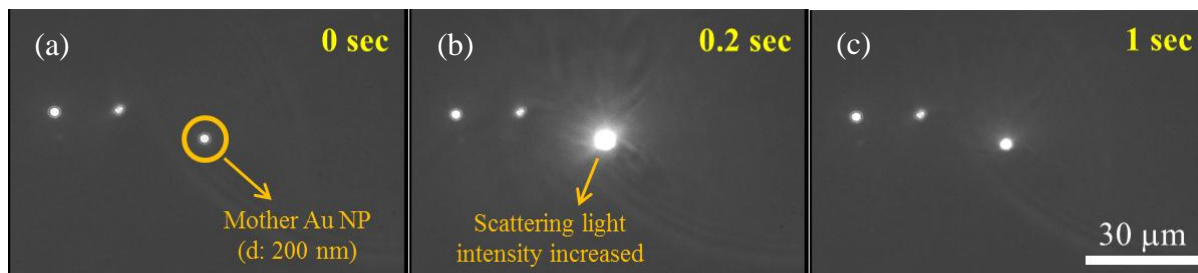


**Fig. 4.1** A series of dark-field scattering images of the mother gold nanoparticle (d: 200 nm) upon a focused laser beam irradiation in fluorescent polystyrene beads (d: 50 nm) solution. The scattering intensity of the mother gold nanoparticle (a) before laser irradiation, (b) during laser irradiation, and (c) after switching off laser by a programmed mechanical shutter after 1 second irradiation. The suspension polystyrene beads are too small to be observed from dark-field image. The laser power, irradiation time, and particle density of solution are 0.5 W, 1 second, and $3.9 \times 10^{11}$ particles/mL, respectively.
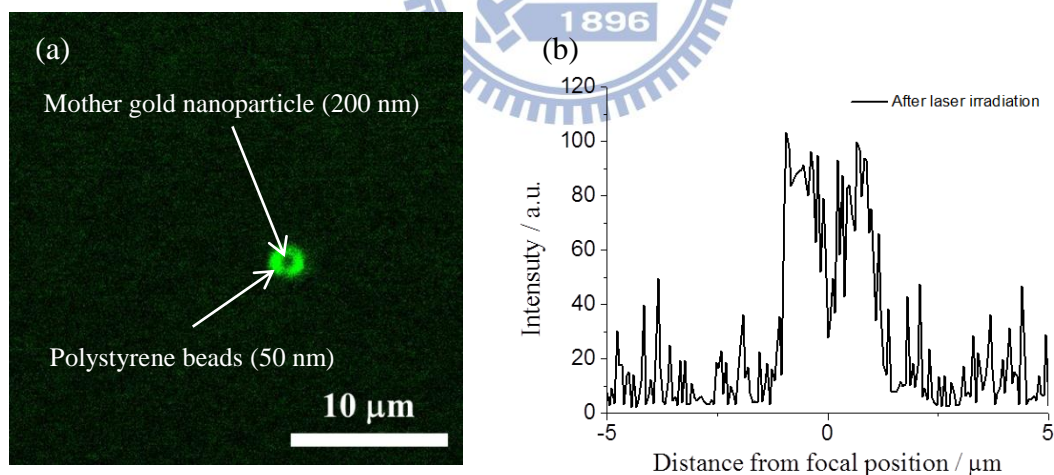


**Fig. 4.2** (a) Fluorescence image shows a doughnut shape of an assembly formation of fluorescent polystyrene beads (d: 50 nm) around the mother gold nanoparticle (d: 200 nm). The hollow center is the position of the mother gold nanoparticle and brighter green signal is the fluorescence intensity of polystyrene. (b) Fluorescence intensity profile gives large intensity around the center.
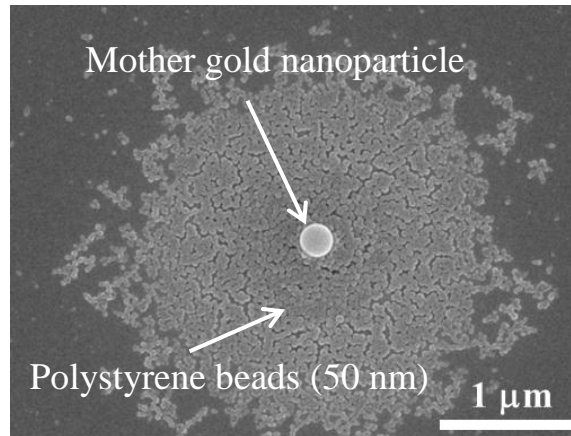
**Fig. 4.3** SEM image of two-dimensional polystyrene beads (d: 50 nm) assembly upon a focused laser beam irradiation on the mother gold nanoparticle (d: 200 nm). The laser power, irradiation time, and particle density of solution are 0.5 W, 1 second, and $3.9 \times 10^{11}$ particles/mL, respectively.

## *4.2.1. Probability of two-dimensional assembly formation*

## *4.2.1.1. Power dependence*

Experimentally, we examined 30 mother gold nanoparticles as the samples under various laser powers with a fixed irradiation time of 1 second. We found that the two-dimensional assembly formation of the polystyrene beads depends on the laser power. The probability of the assembly, defined as the number of assembly divided by the total number of samples done under the same condition, as a function of laser power is shown in Fig. 4.4 (a). In contrary to the assembly formation, we also plot the probability of disappearance, which means that the mother gold nanoparticle evaporated or melted and then detached from substrate. We also repeated the same experiment for the mother gold nanoparticle in pure water solution in the absence of polystyrene beads as reference and the result is shown in Fig. 4.4 (b).
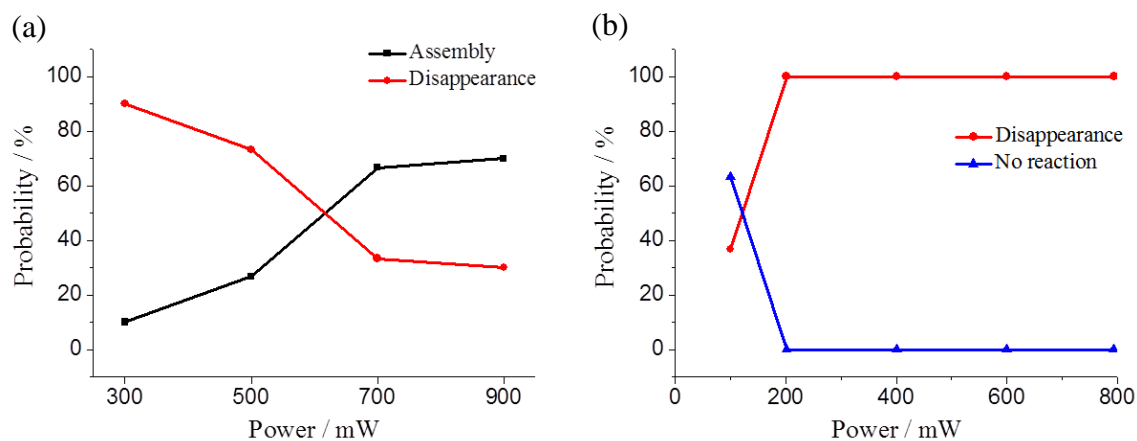
**Fig. 4.4** (a) Probability of polystyrene beads (d: 50 nm) assembly and the mother gold nanoparticle (d: 200 nm) disappearance in fluorescent polystyrene beads solution (particle density is $3.9 \times 10^{11}$ particles/mL). (b) Probability of the mother gold nanoparticle disappearance in pure water solution. The irradiation time was fixed at 1 second.

Fig. 4.4 shows that the assembly probability increases with laser power, in contrast to disappearance that decreases with laser power. We can observe that the disappearance probability of gold nanoparticle is 100% above 200 mW laser power in pure water solution, but suppression of laser-induced evaporation of the mother gold nanoparticle is observed in the solution containing fluorescent polystyrene beads.

## 4.2.1.2. Irradiation time

Since temperature of the mother gold nanoparticle can reach evaporation point due to temperature elevation under long time irradiation, we focus on irradiation time below 1 second as shown in Fig. 4.5 and Fig. 4.6. The irradiation time can be operated at the lowest

time of 0.1 millisecond by using a programmed mechanical shutter. We examined 10 mother

gold nanoparticles as the samples under various irradiation times. We observe that the

probability of assembly fluctuates around the value which corresponds to those obtained in

Fig. 4.4 (a). Such behavior was found under different laser power respectively, and we know

that the time of assembly was quite fast just below than 2 millisecond. The results indicated

that irradiation time dependence of the assembly formation is out of our instrument resolution.
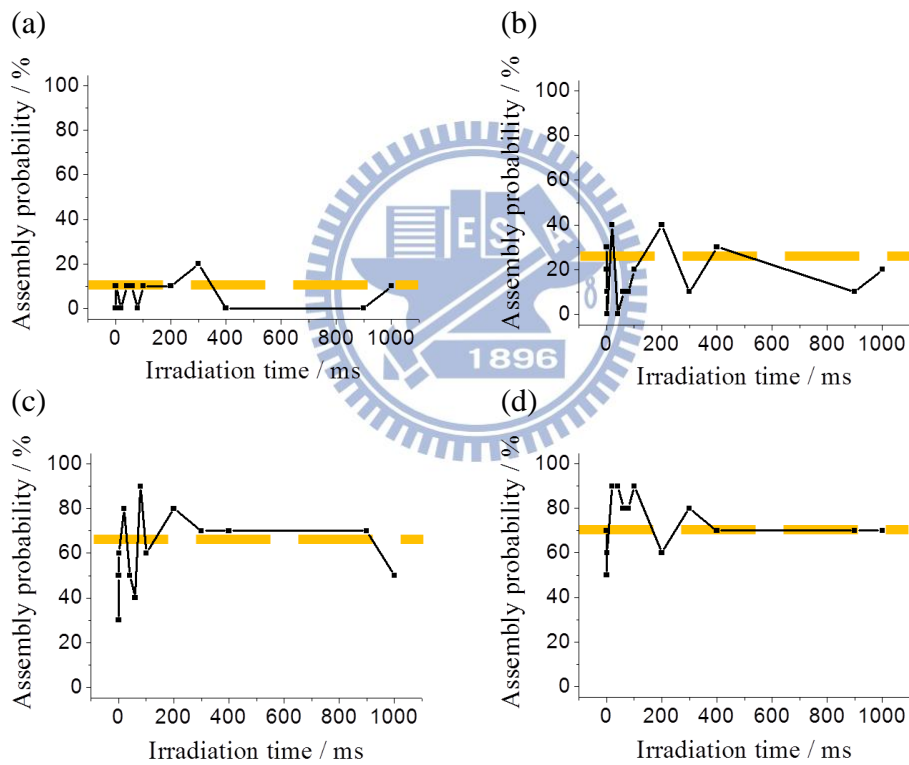


**Fig. 4.5** Irradiation time dependence on assembly probability in suspension fluorescent polystyrene beads solution (particle density is $3.9 \times 10^{11}$ particles/mL) with different laser power (a) 300 mW, (b) 500 mW, (c) 700 mW, and (d) 900 mW from 0.1 to 1000 millisecond irradiation time scale.
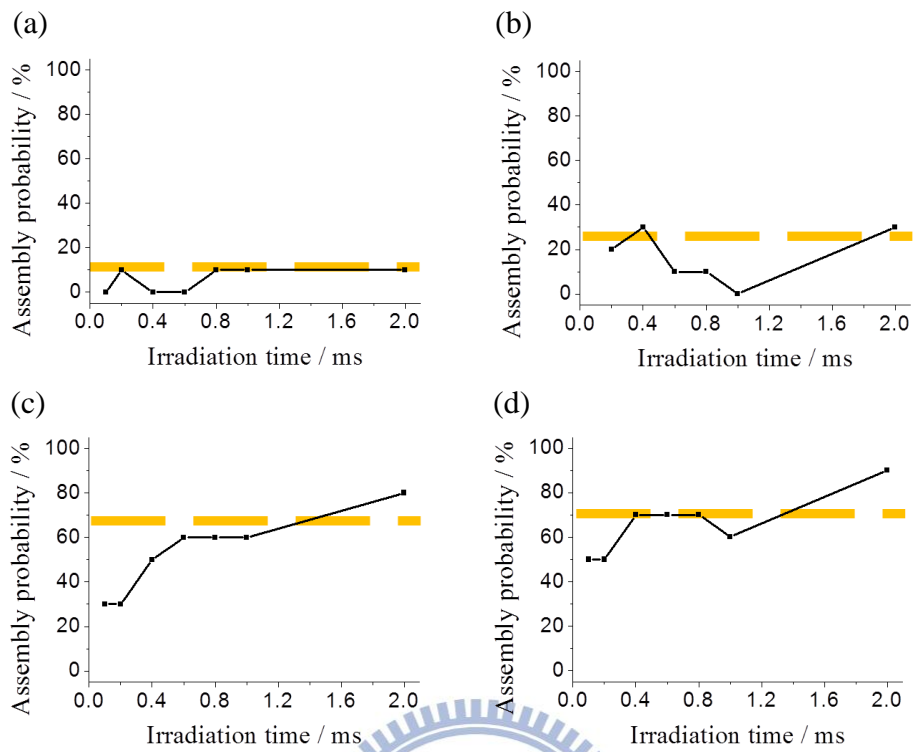
**Fig. 4.6** Irradiation time dependence on assembly probability in suspension of fluorescent polystyrene beads solution (particle density is $3.9 \times 10^{11}$ particles/mL) with different laser power (a) 300 mW, (b) 500 mW, (c) 700 mW, and (d) 900 mW. Here we only focused the time scale from 0.1 to 2 millisecond.

## 4.2.1.3.  Particle density dependence
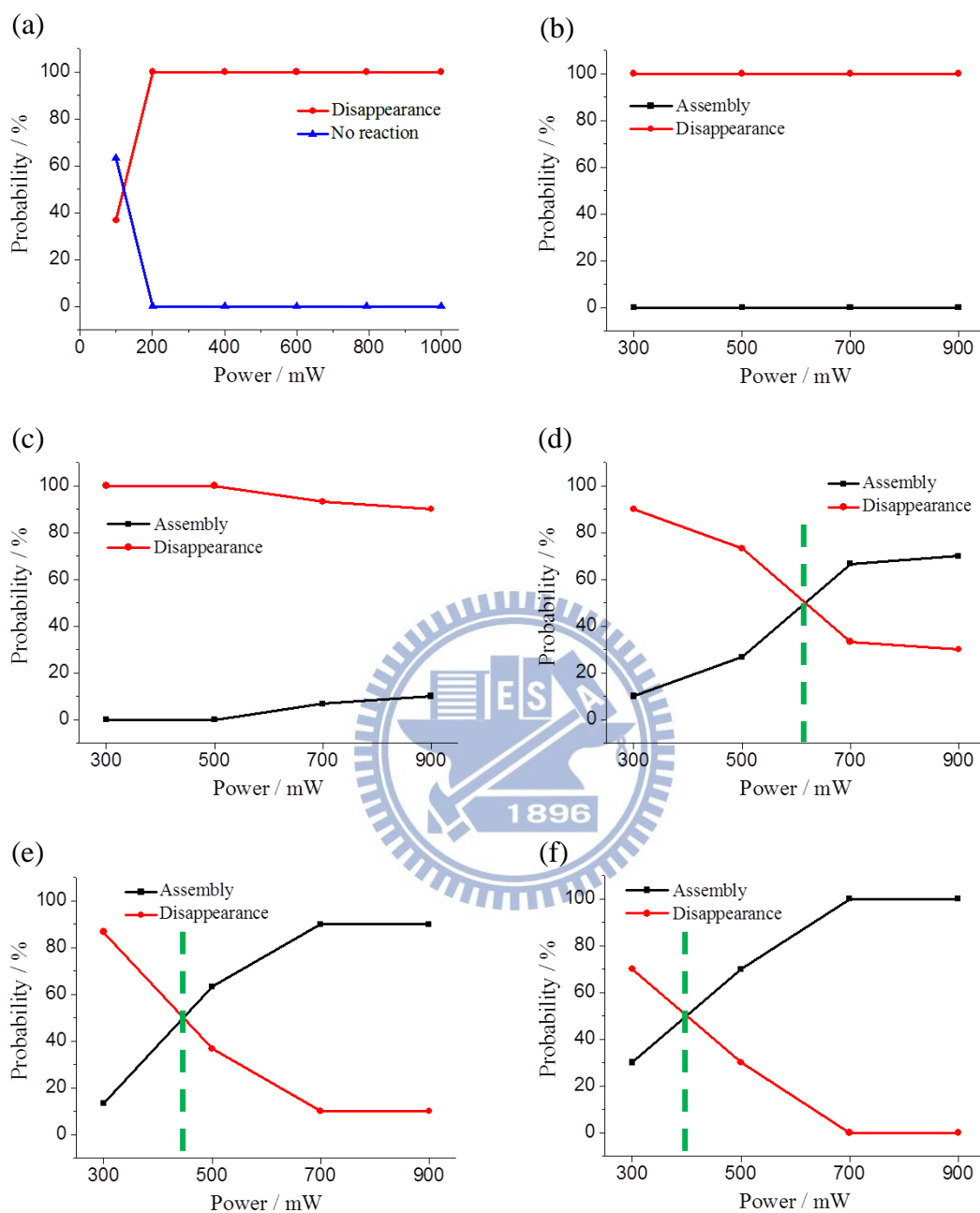


**Fig. 4.7** The assembly probability with various particle density of polystyrene beads solution (a) pure water, (b) $3.9 \times 10^9$, (c) $3.9 \times 10^{10}$, (d) $3.9 \times 10^{11}$, (e) $3.9 \times 10^{12}$ and (f) $3.9 \times 10^{13}$ particles/mL. Green dashed line means laser power where take place at equivalent point of assembly and disappearance probability. The irradiation time was fixed at 1 second.

Fig. 4.7 shows that the assembly probability depends on particle density of polystyrene beads in the solution. Higher particle density means that higher numbers of nanoparticles are gathered around the mother gold nanoparticle. The threshold between assembly and probability shifted to lower laser power when particle density was increased. The shifting down of the threshold as a function of particle density indicates that the mother gold nanoparticle needs more nanoparticles assembled to suppress temperature elevation and to avoid evaporation of the mother gold nanoparticle.

### 4.2.2. Size of two-dimensional assembly

Based on assembly probability results, we know that the assembly formation is induced under various laser power. Therefore, in this section, we focused on the size of two-dimensional formation with various laser powers and did experiments under the same condition as it is in the previous section.

### 4.2.2.1. Power dependence

By SEM observation, we can quantify the size of assembly formation precisely. There are five to ten samples were recorded for each point and the diameter was the average diameter of formed samples assembly for each power, respectively. Fig. 4.9 shows that the

assembly size was increased with incident laser power, indicating that higher laser power can

enlarge heated area and can induce the convection flow more efficiently.
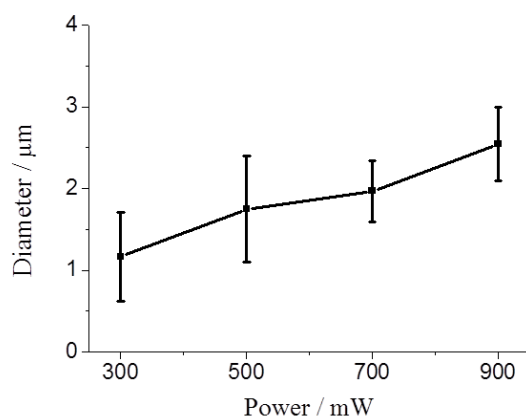


**Fig. 4.8** The size of polystyrene beads assembly formation increased with laser power. The irradiation time and particle density of solution are 1 second and $3.9 \times 10^{11}$ particles/mL, respectively.
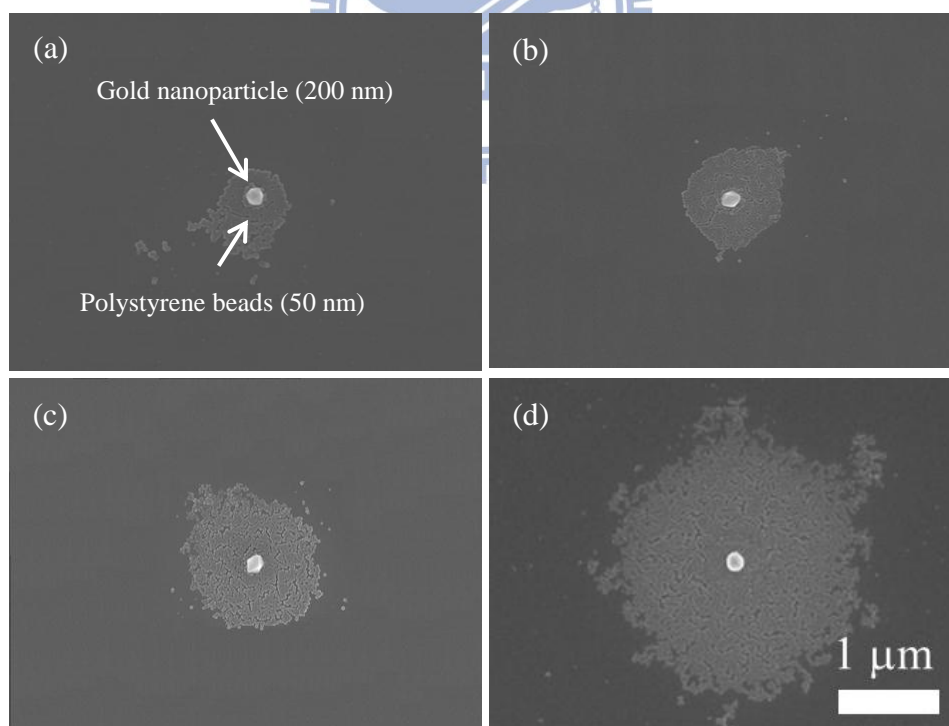


**Fig. 4.9** SEM images of two-dimensional assembly formed at different laser powers (a) 0.3W, (b) 0.5 W, (c) 0.7 W and (d) 0.9 W. The irradiation time and particle density of solution are 1 second and $3.9 \times 10^{11}$ particles/mL, respectively.

## 4.2.2.2. Particle density

In this section, we employed two different particle densities of suspended polystyrene beads solutions of $3.9 \times 10^{12}$ and $3.9 \times 10^{11}$ particles/mL. Fig. 4.10 shows that the assembly size was not depend on particle density obviously, indicating that higher particle density can not affect the assembly size so much in contrast to power effect.
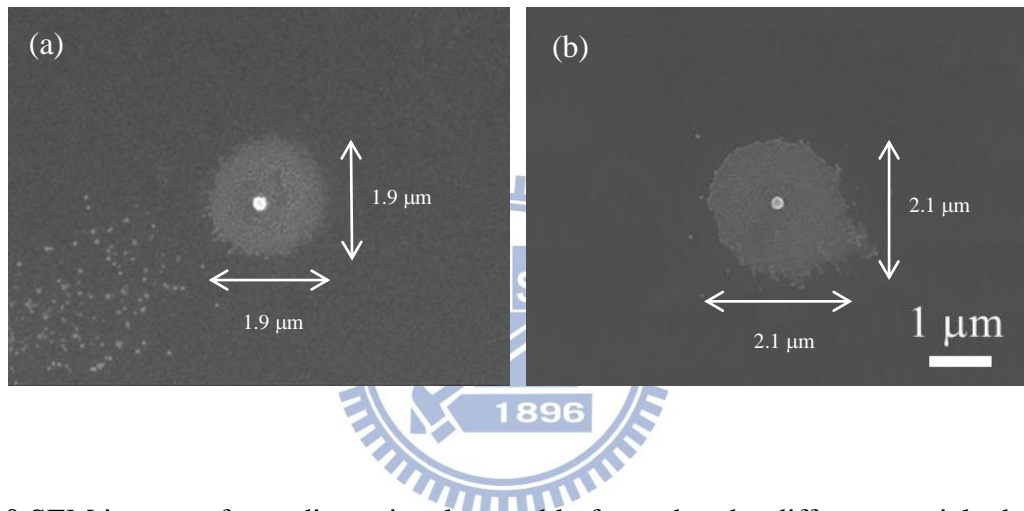


**Fig. 4.10** SEM images of two-dimensional assembly formed under different particle densities, (a) $3.9 \times 10^{12}$ particles/mL and (b) $3.9 \times 10^{11}$ particles/mL, respectively. The laser power and irradiation time are 0.7 W and 1 second, respectively.

## 4.2.2.3. Irradiation time dependence

Since the temperature elevation induced by laser irradiation is time dependent, we focus here on different irradiation time such as 200 milliseconds, 1 second and 2 seconds, respectively. Fig. 4.11 shows that assembly size is increased with irradiation time from 200 milliseconds to 1 second, but the assembly size does not grow up further when the irradiation

time more than 1 second. We can observe that the assembly size is time dependent when irradiation time below 1 second but it is time independent when irradiation time above 1 second.
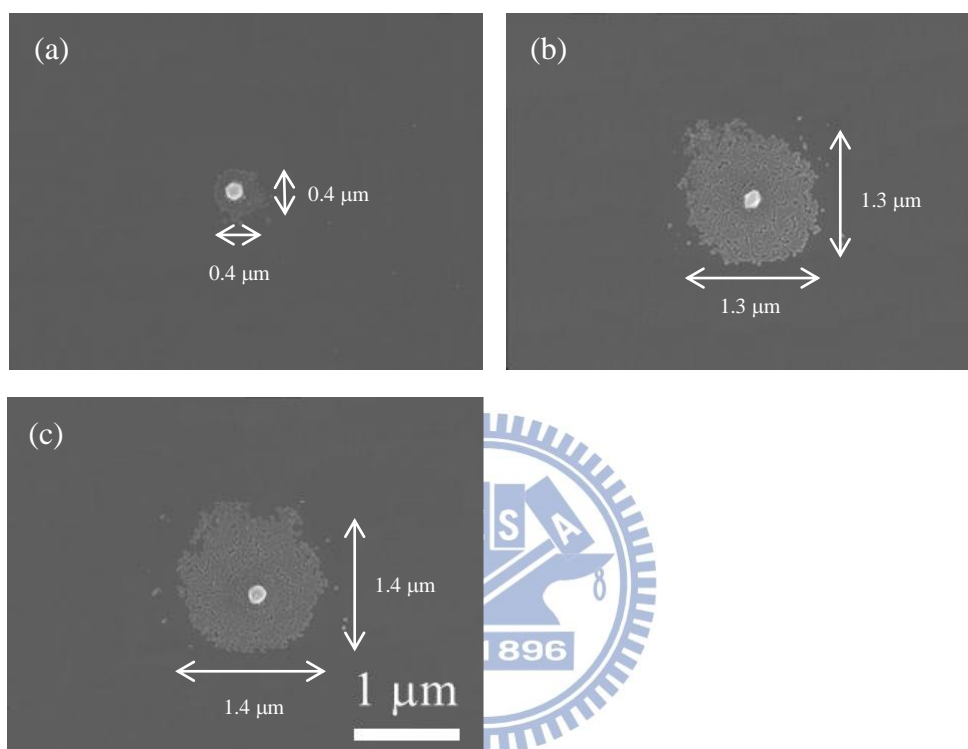


**Fig. 4.11** SEM images of two-dimensional assembly formation at different irradiation times, which are (a) 200 milliseconds, (b) 1 second, and (c) 2 seconds, respectively. The laser power and particle density of solution are 0.5 W and $3.9 \times 10^{11}$ particles/mL, respectively.

## 4.3. Assembly formation of quantum dots, gold nanoparticles, and PNIPAM molecules

Here we applied this method to different materials such as semiconductor (quantum dots) and metallic nanoparticles (gold nanoparticles). We also observe two-dimensional assembly formation upon a focused laser beam on the mother gold nanoparticle in a quantum dots (d: 20 nm) solution similarly to the case of polystyrene beads. The assembly probability, scattering intensity image, and SEM image is shown in Fig. 4.12, Fig. 4.13 and Fig. 4.14, respectively.
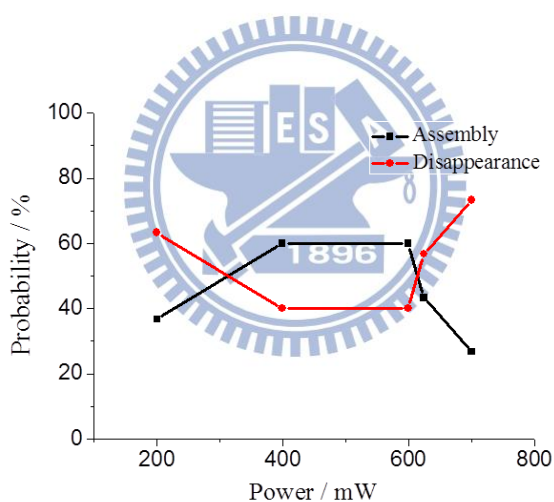


**Fig. 4.12** Probability of quantum dots (d: 20 nm) assembly and the mother gold nanoparticle (d: 200 nm) disappearance in quantum dots solution. The irradiation time and concentration of solution are 1 second and 8 nM, respectively.

**Fig. 4.13** A series of dark-field scattering images of the mother gold nanoparticle (d: 200 nm) upon a focused laser beam irradiation in quantum dots solution. The scattering intensity of the mother gold nanoparticle (a) before laser irradiation, (b) during laser irradiation, and (c) after switching off laser by a programmed mechanical shutter after 1 second irradiation. The suspension quantum dots (d: 20 nm) are too small to be observed from dark-field image. The laser power, irradiation time and concentration of solution are 0.5 W, 1 second and 8 nM, respectively.
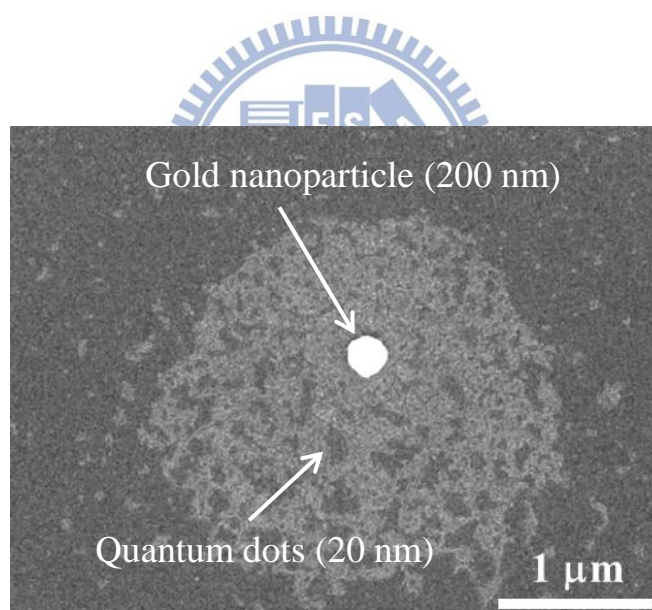


**Fig. 4.14** SEM image of two-dimensional quantum dots (d: 20 nm) assembly upon focused laser beam irradiation on single gold nanoparticle (d: 200 nm). The laser power, irradiation time and concentration of solution are 0.5 W, 1 second and 8 nM, respectively.

We used smaller gold nanoparticles (d: 100 nm) as assembled nanoparticles in solution, and was similarly irradiated the mother gold nanoparticle. The assembly probability is shown in Fig. 4.15. The assembly formation in the gold nanoparticles case shows different phenomena compare with polystyrene beads and quantum dots. Microbubble was formed by focused laser beam heating, as shown in Fig. 4.16. Due to the microbubble formation, we obtained another shape of two-dimensional assembly formation and this rose-like-shaped concentric multiple-rings was shown in Fig. 4.17. The mechanism of these two different types of assembly will be discussed in the next section.
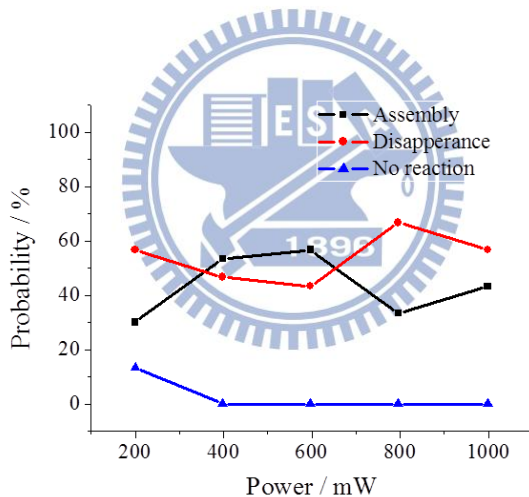


**Fig. 4.15** Probability of gold nanoparticles (d: 100 nm) assembly and the mother gold nanoparticle (d: 200 nm) disappearance in gold nanoparticles solution. The irradiation time and particle density of solution are 1 second and $5.6 \times 10^6$ particles/mL, respectively.
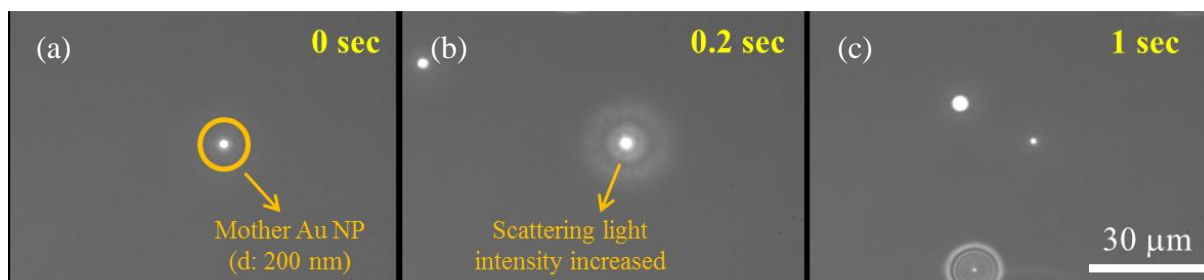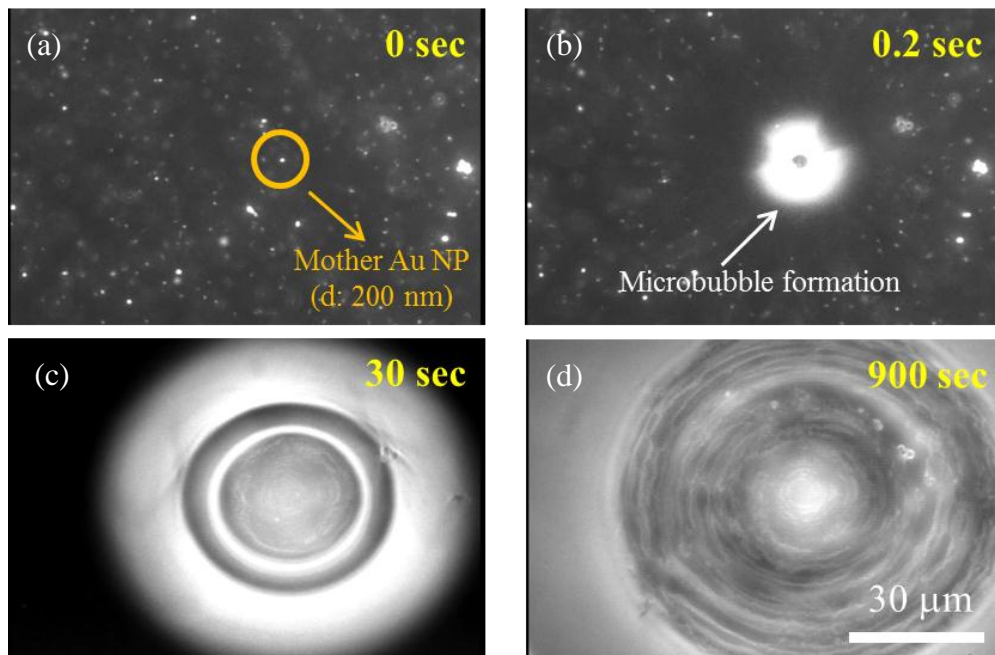
**Fig. 4.16** A series of dark-field scattering images of the mother gold nanoparticle (d: 200 nm) upon a focused laser beam irradiation in gold nanoparticles (d: 100 nm) solution. The scattering intensity of the mother gold nanoparticle (a) before laser irradiation, (b) and (c) during laser irradiation, and (d) after switching off laser by a programmed mechanical shutter after 900 second irradiation. Images of (c) and (d) were taken under reduced intensity of illumination light. The laser power, irradiation time and particle density of solution are 0.5 W, 900 second and $5.6 \times 10^6$ particles/mL, respectively.
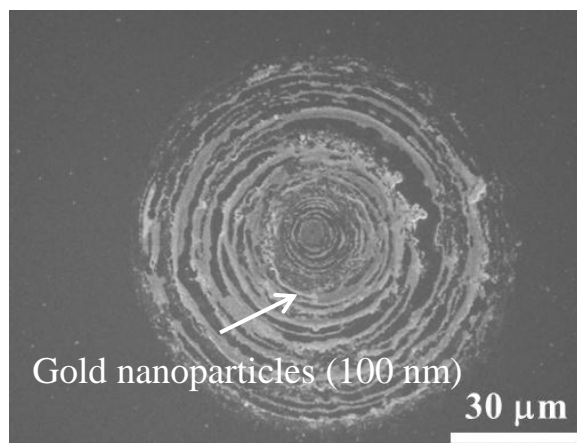


**Fig. 4.17** SEM image of two-dimensional gold nanoparticles (d: 100 nm) assembly upon a focused laser beam irradiation on the mother gold nanoparticle (d: 200 nm). A rose-like multiple-rings structure is formed around the mother gold nanoparticle while the mother gold nanoparticle disappears. The laser power, irradiation time, and particle density of solution are 0.5 W, 900 second and $5.6 \times 10^6$ particles/mL, respectively.

We used poly(N-isopropylacrylamide) (PNIPAM) as assembled nanoparticles in solution, and employed the same laser irradiation for the mother gold nanoparticle. Based on light scattering spectrum and CCD image which shown in Fig. 4.18, we know that PNIPAM assembly around gold nanoparticle after laser irradiation and the heated area increases with laser power. The dark-field observation revealed that PNIPAM molecules exhibited phase transition when they were transported to the vicinity of heated gold nanoparticle. We find the scattering spectrum peak shift to longer wavelength during and after laser irradiation (Fig. 4.18(d)), which indicates that the PNIPAM is gathered on gold nanoparticle surface.
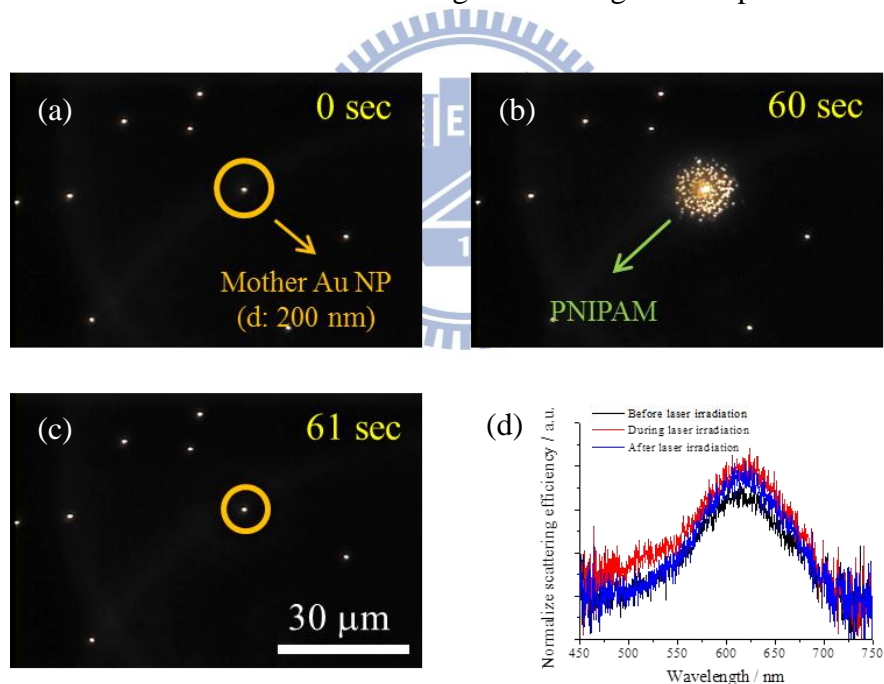


**Fig. 4.18** A series of dark-field scattering images of the mother gold nanoparticle (d: 200 nm) upon a focused laser beam irradiation in PNIPAM solution (500 mg/mL). The scattering intensity of the mother gold nanoparticle (a) before laser irradiation, (b) during laser irradiation, and (c) after switching off laser by a programmed mechanical shutter after 60 second irradiation. The heated suspended PNIPAM near the focal spot can be observed from dark-field image. The laser power, irradiation time and concentration of solution are 0.7 W, 43 second and 200 mg/mL, respectively. (d) The scattering spectra show the intensity changed before, during and after laser irradiation.

According to thermo phase transition of PNIPAM, laser-induced temperature elevation is clearly observed. Then we confirm that the heat transfer from the mother gold nanoparticle to surrounding medium and the heated area are enlarged with laser power, as shown in Fig. 4.19 and Fig. 4.20. The mechanism of PNIPAM assembly also will be discussed in the next section.
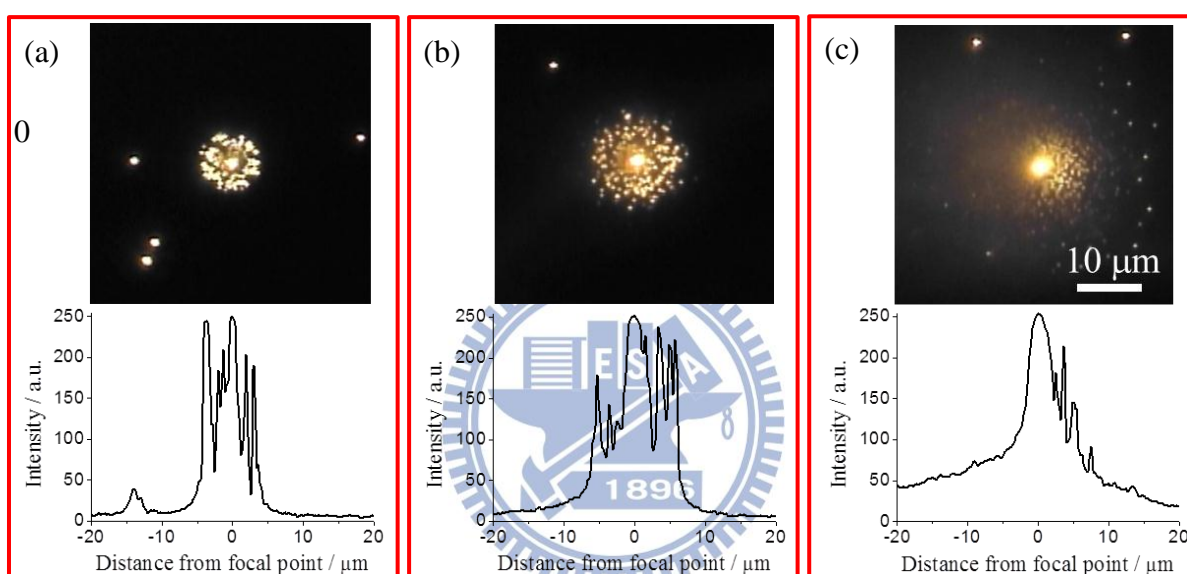


**Fig. 4.19** Dark-field scattering image and scattering light intensity profile with various laser powers (a) 0.3 W, (b) 0.5 W and (c) 0.7 W. The irradiation time and concentration of solution are 40 second and 500 mg/mL, respectively.
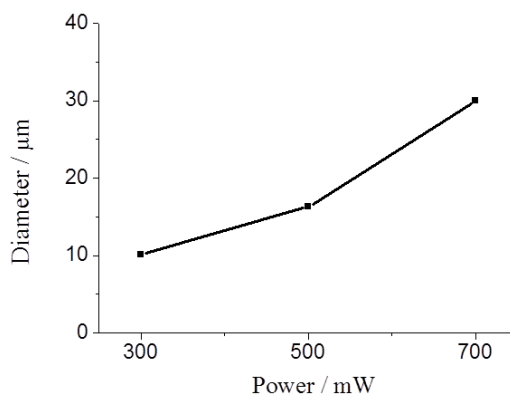


**Fig. 4.20** The size of PNIPAM molecule assembly formation increased with laser power. The irradiation time and concentration of solution are 40 second and 500 mg/mL, respectively.

## 4.4. Discussion

### *4.4.1. Probability of two-dimensional assembly formation*

The result presented in previous section reveals that the assembly probability depends on laser power and particle density. A higher laser power enhanced heated area from focused position to surrounding medium and induced convection flow not only broader but also more efficiently, while higher particle density meant much more nanoparticles at near the focused spot. Larger heated area and higher particle density contributes to accumulate nanoparticle efficiently and suppresses the evaporation of heated mother gold nanoparticle due to temperature elevation. Based on the result, we know that temperature reaches an equilibrium within less than 0.1 millisecond, and then convection flow and assembly formation are induced simultaneously. Therefore, the assembly of nanoparticles is formed efficiently within a short irradiation time, and laser power and particle density are the main factors governing the probability of the assembly formation.

### *4.4.2. Size of two-dimensional assembly*

According to our results, the assembly size depends on laser power obviously and not depends on particle density. From the above section, we know that the laser power affect not only assembly probability but also assembly size, due to higher laser power enlarged heated area and induced convection flow more efficiently. From Fig. 4.10, we know that particle

density does not affect assembly size markedly but assembly probability obviously. It strongly

suggests that suppression of temperature elevation does not depend on numbers of assembly

nanoparticles dominantly but depends on numbers of suspended nanoparticles in the vicinity

around the mother gold nanoparticle. Therefore, the results show particle density dependence

of assembly probability but not of assembly size. The assembly size increases with irradiation

time till 1 second but stops to grow over 1 second. Therefore, laser power and irradiation time

are the main factors of nanoparticles assembly size.

### *4.4.3. Two-dimensional assembly formation mechanism*

For polystyrene beads, quantum dots and PNIPAM molecules, we observed

two-dimensional assembly around the mother gold nanoparticle as typically shown in Fig. 4.3,

Fig. 4.14 and Fig. 4.19. Since the assembly size is much larger than that of the laser spot,

convection flow generated near the gold nanoparticles should contribute to the nanoparticles

accumulation. On the other hand, in the case of gold nanoparticles assembly, they form

concentric multiple-rings structure around the irradiated mother nanoparticle while the mother

nanoparticle disappeared as exhibited in Fig. 4.17. It is noteworthy that thermal bubbling is

observed at the laser focus during the accumulation only in this case. This strongly suggests

that photoabsorption and energy dissipation modes depend on the coupling of the mother gold

nanoparticle and gathered nanoparticles, leading to different accumulation and structure

formation.

Photothermal heating of gold nanoparticle and heat transfer to medium take place upon focused laser beam irradiation on the mother gold nanoparticle. Then, temperature gradient induced by heat transfer from the mother gold nanoparticle with local heating to surrounding medium leads convection flow. Heat-induced convection flow results in mass transfer toward the heated position. Suspended nanoparticles in solution were drawn toward to the mother gold nanoparticle via convection flow and formed assembly around the mother gold nanoparticle. The nanoparticles are fixed on substrate through electrostatic force between nanoparticles and substrate. The nanoparticles were adhered strongly on the substrate after removing solution, the result indicate that the binding of the nanoparticles to substrate is quite stable. The assembly formation of these two different mechanisms was shown in Fig. 4.21, Fig. 4.22 and Fig. 4.23, respectively.
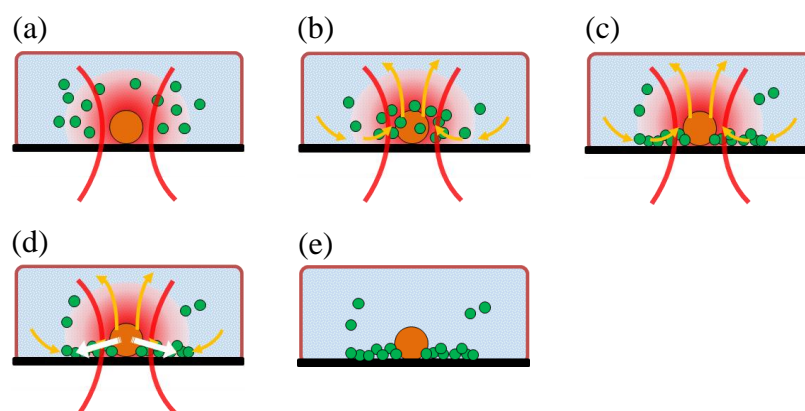


**Fig. 4.21** The schematic illustration of the assembly formation mechanism in the cases of polystyrene beads and quantum dots. (a) Photo-thermal heating of the mother gold

nanoparticle by focused laser beam and heat transfer to surrounding medium. (b) Convection flow was induced due to temperature gradient by laser heating and drew nanoparticles toward to the mother gold nanoparticle. (c) Nanoparticles adsorbed on the mother gold nanoparticle, giving two-dimensional assembly. (d) Heat transfer from the mother gold nanoparticle to surrounding medium suppressed the former temperature elevation leading to no evaporation. (e) After switching off laser, nanoparticles assembly formation was finished.
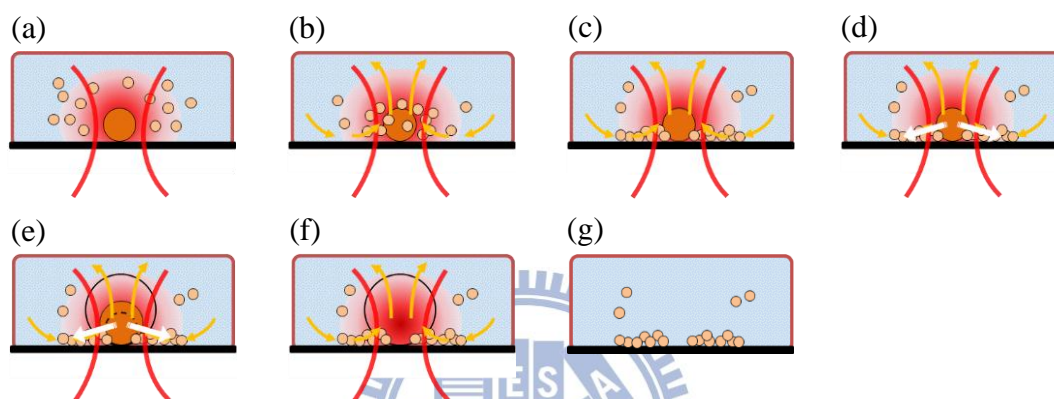


**Fig. 4.22** The schematic illustration of the assembly formation mechanism in the case of gold nanoparticles. (a) Photo-thermal heating of the mother gold nanoparticle by focused laser beam and heat transfer to surrounding medium. (b) Convection flow was induced due to temperature gradient by laser heating and drew nanoparticle toward to the mother gold nanoparticle. (c) Gold nanoparticles were adsorbed on the mother gold nanoparticle, giving two-dimensional assembly. (d) Heat transfer from the mother gold nanoparticle to surrounding medium suppressed the former temperature elevation leading to no evaporation. (e) Fusion of gold nanoparticles enhanced temperature elevation efficiently and formed a microbubble on the mother gold nanoparticle surface. (f) Temperature elevated efficiently near focused spot led to evaporation of the mother gold nanoparticle, inducing wider heated area and forming the microbubble. Due to the microbubble formation, we obtained concentric shape of the two-dimensional assembly. (g) After switching off laser, nanoparticles assembly formation was finished, while the mother gold was not observed anymore.
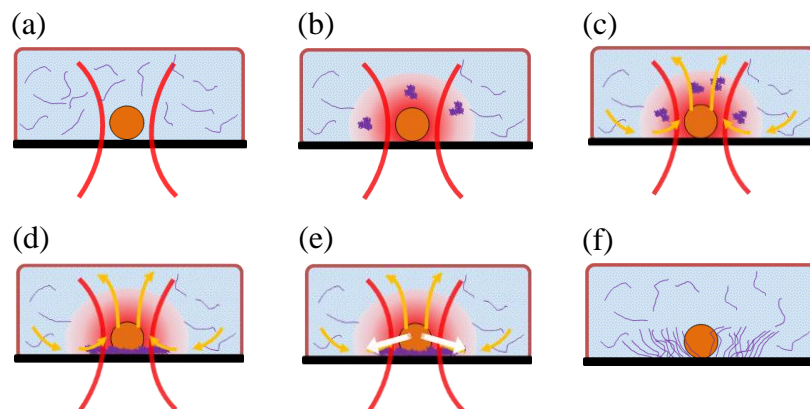
**Fig. 4.23** The schematic illustration of the assembly formation mechanism in the case of PNIPAM molecules. (a) (b) Photo-thermal heating of the mother gold nanoparticle by focused laser beam and heat transfer to surrounding medium. PNIPAM has phase transition to globule at heated area. (c) Convection flow was induced due to temperature gradient by laser heating, and PNIPAM comes to heated area around the mother gold nanoparticle via convection flow and goes phase transition giving globule conformation. (d) PNIPAM molecules were adsorbed on the mother gold nanoparticle, and forming two-dimensional assembly. (e) Heat transfer from the mother gold nanoparticle to surrounding medium suppressed the former temperature elevation leading to no evaporation. (f) After switching off laser, PNIPAM molecules assembly formation was finished and the globule conformation comes back to coil one upon temperature lowering.

## 4.5. Summary

In this work, upon CW laser irradiation on the single mother gold nanoparticle, we succeeded in forming two-dimensional nanoparticles assembly in the vicinity of the mother nanoparticle though the assembly structure is different depending on the nanoparticle materials. The CW laser-heated induced assembly formation of the different kinds of nanoparticles has been studied in detail by changing various experimental parameters. Here we can propose optimized parameters to improve the assembly probability and size.

# Chapter 5

# Comparison to Calculation

In this section, we concentrate on the relation between experimental and numerically calculated results. Based on Mie theory, which we explained in Chapter 2, we could calculate the absorption cross section of various gold nanoparticles size and the adsorption spectra of gold nanoparticles by solving Eq. 9, and the calculated absorption cross section was shown in Fig. 5.1, where $\varepsilon_m$ is 1.4, and gold nanoparticle radius $a$ is 100 nm. According to the calculation, it is obvious that absorption cross section of gold nanoparticle increases with particle size, and it shows that the maximum plasmon resonance wavelength of gold nanoparticle is around 532-nm. Here we used 1064-nm laser irradiation as light source to avoid highly temperature elevation due to strong light adsorption at 532-nm.
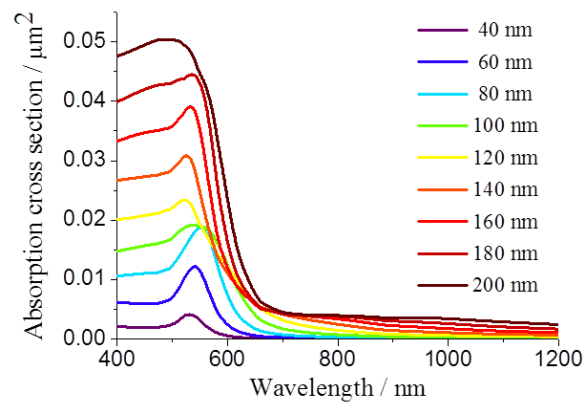


**Fig. 5.1** Size dependent absorption cross section spectra of gold nanoparticles.

From Eq. 16, we could calculate the temperature of gold nanoparticle and the results was

shown in Fig. 5.2, where the laser wavelength is 1064-nm, numerical aperture of objective

lens is 0.9, refractive index of medium is 1.4, heat conductivity of water is 0.6  W/m·K, and

room temperature is 293 K. The temperature elevates quite efficiently for a larger gold

nanoparticle due to higher adsorption cross section.
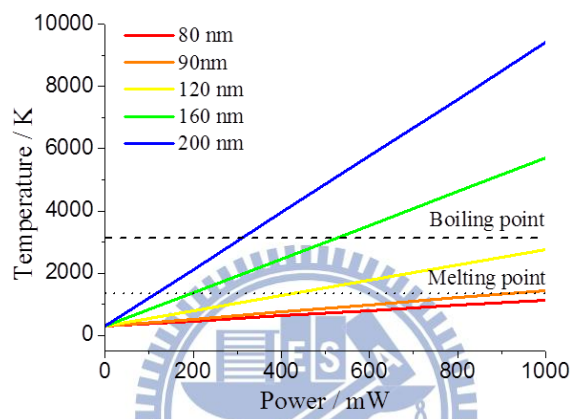


**Fig. 5.2** Temperature elevation of gold nanoparticle under illumination of 1064-nm laser beam.
The laser wavelength is 1064-nm, numerical aperture of objective lens is 0.9, refractive index
of medium is 1.4, heat conductivity of water is 0.6  W/m·K, and room temperature is 293 K.

The additional result is shown in Fig. 5.3 and Fig. 5.4, in which we observe that the size

of gold nanoparticles decreased by laser irradiation in pure water solution. In spite of the

different initial sizes (which in within orange dashed line rectangle) of gold nanoparticles, 100

nm and 200 nm, all the final sizes are below the threshold around 90 nm. The additional

information indicates that the final reduced sizes are independent on laser power. To compare

with the calculation, it was assumed that the gold nanoparticle is heated by laser and then that

temperature is enhanced. Size reduction of gold nanoparticle decreases the temperature to the

range below the melting point (1337K).
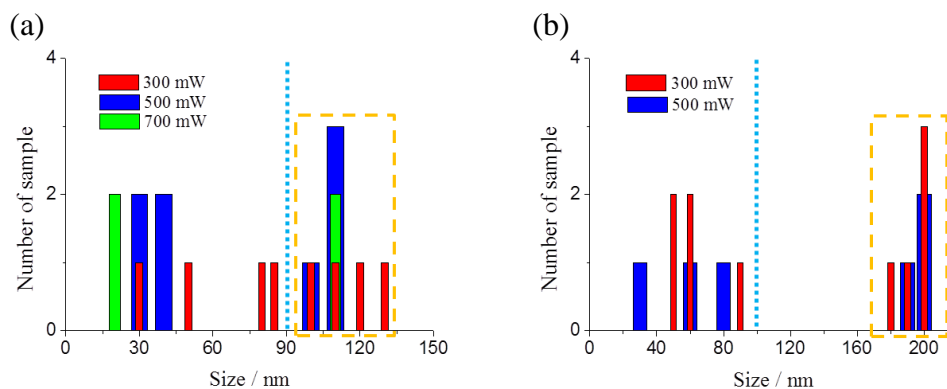


**Fig. 5.3** Size distribution of examined mother gold nanoparticles. Inside the orange dashed region are the initial sizes. Below the blue dotted line are the sizes after laser irradiation; (a) for nominal 100 nm and (b) for nominal 200 nm. The final size of the mother gold nanoparticle is always below 90 nm. We determined the size of the target gold nanoparticle by means of the light scattering spectrum, and the spectrum was fitted by calculation based on Mie theory. With this method, we could check the size reduction of target gold nanoparticle before and after laser irradiation directly.
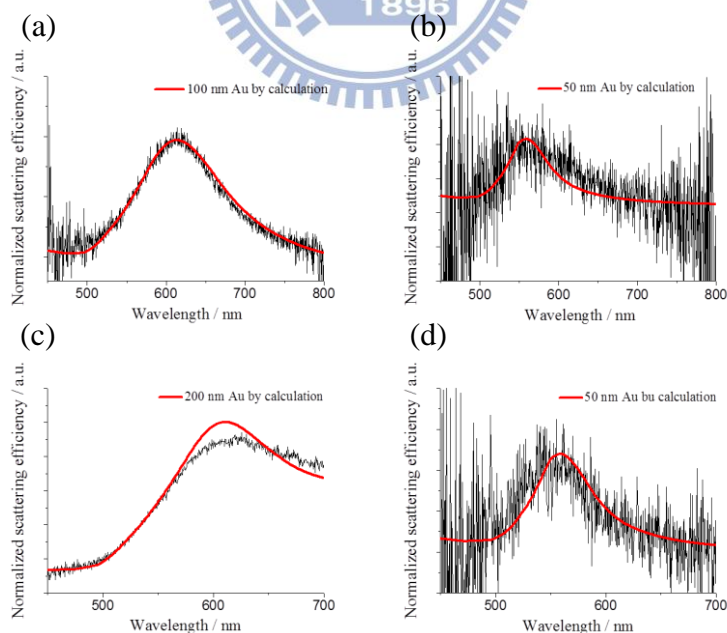


**Fig. 5.4** The scattering light efficiency of the mother gold nanoparticle before laser irradiation (a) 100 nm and (c) 200 nm. (b) and (d) show the scattering light efficient of the mother gold nanoparticle after 1 second laser irradiation of (a) and (c), respectively. The red line was calculated based on Mie theory and the experiment was carried out in pure water solution.

According to the result of PNIPAM, we observed that the heated area increases with laser power. Based on Eq. 16, we could calculate the radial temperature-change distribution from gold nanoparticle surface to surrounding medium (water) and the calculation was shown in Fig. 5.5. The temperature decrease with the distance from gold nanoparticle surface to water and it steeply falls in the surrounding medium. The radial temperature profile reveals that the temperature falls more rapidly for a smaller gold nanoparticle size. Based on Mie theory predictions, an absorption cross section rapidly increases with particle size due to larger polarizability.

**Fig. 5.5** Size dependent heat transfer to surrounding medium.

Temperature elevation of gold nanoparticle results in heat transfer to the medium, inducing convection flow. Therefore, suspended nanoparticles in solution assembled around the mother gold nanoparticle via convection flow could be observed.

# Chapter 6

# Conclusion

In this study, we have demonstrated two-dimensional assembly formation on glass substrate of various nanoparticles suspended in aqueous solution by temperature elevation upon tightly focused laser irradiation on the mother gold nanoparticle spin-coated on the glass substrate. For polystyrene beads or quantum dots, two-dimensional assembly i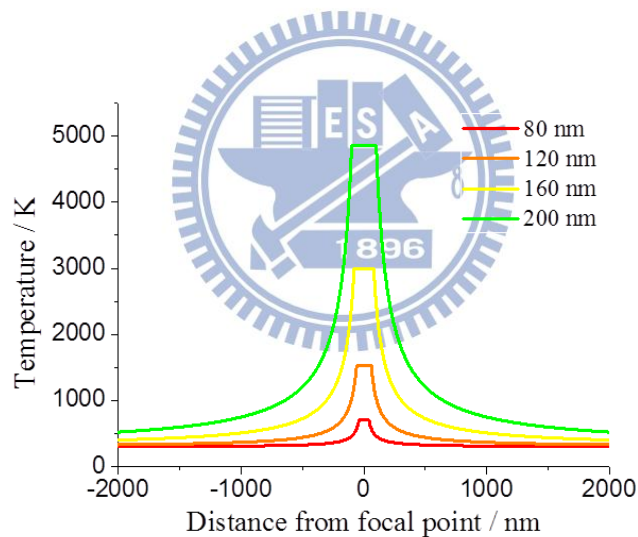s formed around the mother gold nanoparticle. In the case of gold nanoparticles assembly, they form concentric multiple-rings structure around the focused mother nanoparticle while the mother nanoparticle disappears. From SEM images, it is clarified that two-dimensional assembly of nanoparticles was formed in the vicinity of the mother gold nanoparticle.

We explored how laser irradiation parameters, such as laser power, irradiation time, and particle density of suspended nanoparticles in solution affect assembly probability and obtained size, and then we proposed optimized parameters to improve the assembly probability and size. A larger heated area enhances the efficiency of convection flow, allowing us to control the size of assembly area with varying laser power. More suspended nanoparticles in the vicinity around the focal spot suppress the temperature of the mother gold nanoparticle more efficiently to avoid evaporation, allowing us to control the assembly probability with different particle density. Convection flow induced by local heating, in this

study, does not depend on optical/electric/magnetic properties of the suspended nanoparticles,

and thus this method would open new vistas for applications of the two-dimensional assembly

formation of the nanoparticles.

# References

1.  K. Christmann, et al., "Chemisorption geometry of hydrogen on Ni(111): Order and disorder", <u>J. Chem. Phys.</u>, **70**(9), 4168-4184 (1979)

2.  M. Prutton, <u>Introduction to surface physics</u>, Oxford University Press, USA, 1994

3.  K. Bogunia-Kubik and M. Sugisaka, "From molecular biology to nanotechnology and nanomedicine", <u>BioSyst.</u>, **65**(2–3), 123-138 (2002)

4.  W.T. Astbury, "Molecular Biology or Ultrastructural Biology ?", <u>Nature</u>, **190**(4781), 1124-1124 (1961)

5.  M. Sarikaya, et al., "Molecular biomimetics: nanotechnology through biology", <u>Nat. Mater.</u>, **2**(9), 577-85 (2003)

6.  B.H. Cumpston, et al., "Two-photon polymerization initiators for three-dimensional optical data storage and microfabrication", <u>Nature</u>, **398**(6722), 51-54 (1999)

7.  H.-B. Sun and S. Kawata, "Two-Photon Photopolymerization and 3D Lithographic Microfabrication", 169-273 (2004)

8.  S.K. Sahoo and V. Labhasetwar, "Nanotech approaches to drug delivery and imaging", <u>Drug Discovery Today</u>, **8**(24), 1112-1120 (2003)

9.  S.-L. Lin, et al., "Microfluidic chip-based liquid chromatography coupled to mass spectrometry for determination of small molecules in bioanalytical applications", <u>Electrophoresis</u>, **33**(4), 635-643 (2012)

10. V. Srinivasan, V.K. Pamula, and R.B. Fair, "An integrated digital microfluidic lab-on-a-chip for clinical diagnostics on human physiological fluids", <u>Lab on a Chip</u>, **4**(4), 310-315 (2004)

11. G. Meyer, et al., "Controlled Manipulation of Atoms and Small Molecules with a Low Temperature Scanning Tunneling Microscope", <u>Single Molecules</u>, **1**(1), 79-86 (2000)

12. T. Junno, et al., "Controlled manipulation of nanoparticles with an atomic force microscope", <u>Appl. Phys. Lett.</u>, **66**(26), 3627-3629 (1995)

13. Y. Xia, et al., "Unconventional Methods for Fabricating and Patterning Nanostructures", <u>Chem. Rev.</u>, **99**(7), 1823-1848 (1999)

14. I.W. Hamley, "Nanostructure fabrication using block copolymers", <u>Nanotechnology</u>, **14**(10), R39 (2003)

15. M.C. Buncick, R.J. Warmack, and T.L. Ferrell, "Optical absorbance of silver ellipsoidal particles", <u>J. Opt. Soc. Am. B</u>, **4**(6), 927-933 (1987)

16. S. Hayashi, et al., "Imaging by polystyrene latex particles", <u>J. Colloid Interface Sci.</u>, **144**(2), 538-547 (1991)

17. F. Lenzmann, et al., "Thin-film micropatterning using polymer microspheres", <u>Chem.</u>

Mater., **6**(2), 156-159 (1994)

18. F. Burmeister, et al., "Colloid Monolayers as Versatile Lithographic Masks", Langmuir, **13**(11), 2983-2987 (1997)

19. N.D. Denkov, et al., "Two-dimensional crystallization", Nature, **361**(6407), 26-26 (1993)

20. S. Liu, et al., "Evaporation-induced self-assembly of gold nanoparticles into a highly organized two-dimensional array", PCCP, **4**(24), 6059-6062 (2002)

21. I.U. Vakarelski, C.E. McNamee, and K. Higashitani, "Deposition of silica nanoparticles on a gold surface via a self-assembled monolayer of (3-mercaptopropyl)trimethoxysilane", Colloids Surf. Physicochem. Eng. Aspects, **295**(1–3), 16-20 (2007)

22. A. Ashkin, "Acceleration and Trapping of Particles by Radiation Pressure", Phys. Rev. Lett., **24**(4), 156-159 (1970)

23. A. Ashkin, et al., "Observation of a single-beam gradient force optical trap for dielectric particles", Opt. Lett., **11**(5), 288-290 (1986)

24. A. Ashkin, "Forces of a single-beam gradient laser trap on a dielectric sphere in the ray optics regime", Biophys. J., **61**(2), 569-582 (1992)

25. A. Ashkin, "Optical trapping and manipulation of neutral particles using lasers", Proc. Natl. Acad. Sci. U.S.A., **94**(10), 4853-4860 (1997)

26. K.C. Neuman and S.M. Block, "Optical trapping", Rev. Sci. Instrum., **75**(9), 2787-2809 (2004)

27. D. Erenso, et al., "Formation of synthetic structures with micron size silica beads using optical tweezer", J. Mod. Opt., **54**(10), 1529-1536 (2007)

28. S. Fujii, et al., "Observation of DNA pinning at laser focal point on Au surface and its application to single DNA nanowire and cross-wire formation", Bioelectrochemistry, **80**(1), 26-30 (2010)

29. S. Fujii, et al., "Manipulation of Single DNA Using a Micronanobubble Formed by Local Laser Heating on a Au-coated Surface", Chem. Lett., **39**(2), 92-93 (2010)

30. S. Fujii, et al., "Fabrication and Placement of a Ring Structure of Nanoparticles by a Laser-Induced Micronanobubble on a Gold Surface", Langmuir, **27**(14), 8605-8610 (2011)

31. T. Uwada, et al., "Glycine Crystallization in Solution by CW Laser-Induced Microbubble on Gold Thin Film Surface", ACS Appl. Mater. Interfaces, **4**(3), 1158-1163 (2012)

32. Y. Seol, A.E. Carpenter, and T.T. Perkins, "Gold nanoparticles: enhanced optical trapping and sensitivity coupled with significant heating", Opt. Lett., **31**(16), 2429-2431 (2006)

33. R.W. Wood, "On a Remarkable Case of Uneven Distribution of Light in a Diffraction

Grating Spectrum", <u>Proc. Phys. Soc. London</u>, **18**(1), 269 (1902)

34. G. Mie, "Beiträge zur Optik trüber Medien, speziell kolloidaler Metallösungen", <u>Annalen der Physik</u>, **330**(3), 377-445 (1908)

35. C.K. Chen, et al., "Surface-enhanced second-harmonic generation and Raman scattering", <u>Phys. Rev. B</u>, **27**(4), 1965-1979 (1983)

36. M. Moskovits, "Surface-enhanced spectroscopy", <u>Rev. Mod. Phys.</u>, **57**(3), 783-826 (1985)

37. B. Nikoobakht, J. Wang, and M.A. El-Sayed, "Surface-enhanced Raman scattering of molecules adsorbed on gold nanorods: off-surface plasmon resonance condition", <u>Chem. Phys. Lett.</u>, **366**(1–2), 17-23 (2002)

38. X. Qian, et al., "In vivo tumor targeting and spectroscopic detection with surface-enhanced Raman nanoparticle tags", <u>Nat Biotech</u>, **26**(1), 83-90 (2008)

39. K.L. Kelly, et al., "The Optical Properties of Metal Nanoparticles: The Influence of Size, Shape, and Dielectric Environment", <u>J. Phys. Chem. B</u>, **107**(3), 668-677 (2002)

40. P. Keblinski, et al., "Limits of localized heating by electromagnetically excited nanoparticles", <u>J. Appl. Phys.</u>, **100**(5), 054305 (2006)

41. E.J.G. Peterman, F. Gittes, and C.F. Schmidt, "Laser-Induced Heating in Optical Traps", <u>Biophys. J.</u>, **84**(2), 1308-1316 (2003)

42. R. Bhargara, "Properties of Wide Bandgap II—VI Semiconductors", <u>Cryst. Res. Technol.</u>, **33**(5), 706-706 (1998)

43. M. Arzberger and M.C. Amann, "Homogeneous line broadening in individual semiconductor quantum dots by temperature fluctuations", <u>Phys. Rev. B</u>, **62**(16), 11029-11037 (2000)

44. A. Pashinkin, et al., "Heat capacity of solid A$^{II}$Se and A$^{II}$Te above 298 K", <u>Inorg. Mater.</u>, **48**(1), 28-33 (2012)

45. M. Vieweger, et al., "Photothermal Imaging and Measurement of Protein Shell Stoichiometry of Single HIV-1 Gag Virus-like Nanoparticles", <u>ACS Nano</u>, **5**(9), 7324-7333 (2011)

46. C.A. Estrada-Gasca, et al., "Theoretical efficiency of an all-glass tubular solar collector using a chemically deposited SnS-Cu x S absorber inside the inner tube", <u>J. Phys. D: Appl. Phys.</u>, **25**(7), 1142 (1992)

47. R. Kato, A. Maesono, and R.P. Tye, "Thermal Conductivity Measurement of Submicron-Thick Films Deposited on Substrates by Modified ac Calorimetry (Laser-Heating Å ngstrom Method)", <u>Int. J. Thermophys.</u>, **22**(2), 617-629 (2001)